tients with postoperative predicted $FEV_{1.0}$ ≥800 ml, PaO_2 ≥65 torr, absent severe cardiac/heart disease, and absent severe diabetes mellitus; 2) inoperable patients who do not satisfy the criteria for operable patients.

The treatment consists of 48 Gy in four fractions over 4 to 8 days. The prescription point is the isocenter, and the monitor units are calculated with heterogeneity correction. The Clarkson integration algorithm is used, and the convolution-superposition algorithm is not allowed in this study.

In treatment planning, the clinical target volume (CTV) was defined as the gross tumor volume (GTV). An internal margin according to each institution was added to the CTV to define the internal target volume (ITV). The planning target volume (PTV) was defined as the ITV plus 5 mm of setup margin. The radiation ports were set to the PTV with 5 mm of leaf margin. Non-coplanar static beams (5 to 10 ports) or multiple-arc beams (in total ≥400 degrees) with 4 to 10 MV X-rays are allowed. Dose constraints to normal tissues, i.e. the lung, the esophagus, the bronchial tree, the great vessels, the spinal cord, are also defined.

QUALITY CONTROL AND QUALITY ASSURANCE

Quality control (QC) and quality assurance (QA) for radiotherapy in multicenter clinical trials are vital to evaluate new investigational treatments. In contrast to the United States, where a QC/QA program was developed in the late 1960s, it was not developed in the 20th century in Japan. In 2001, we performed a retrospective final review using a JCOG trial for the first time,[10,11] and it revealed that protocol compliance was very poor, with a protocol violation rate of 60%. After these results, we developed the Radiotherapy Quality Assurance Center (RTQAC) in the JCOG and started a comprehensive QC/QA program, including individual case reviews (initial and final reviews). The first trial with a QC/QA program was opened for accrual in 2002. Protocol violation has been decreasing yearly, and it is now less than 5%.

In the JCOG 0403 study, we asked the National Cancer Institute and the Advanced Technology Consortium (ATC) to support this trial in developing a QC/QA program. The digital data of each case from radiotherapy planning systems are submitted to the Image Guided Therapy QA Center (ITC) at Washington University in St. Louis, and the final review is being performed using the Remote Review Tool provided by the ITC.

In 2004, we also developed a non-profit organization, the Radiotherapy Support Center (RSC) to support QC/QA activities in clinical trials. The RSC, instead of the RTQAC, is now charged with radiotherapy QC/QA in JCOG trials.

CREDENTIAL PROCESS

Participating institutions in the JCOG 0403 study must pass through the following requirements: 1) a survey of institutional personnel, equipment, and treatment techniques; 2) dry run; and 3) phantom dosimetry test. An institutional survey includes immobilization/localization precision. They are required to present a document that shows the setup reproducibility for their choice of immobilization and/or localization equipment.

A dry run must be performed to reduce inter-institutional variations of treatment planning in compliance with the protocol and to check the institutional capability of digital data submission to the ATC. The results of the dry run performed before the JCOG 0403 study will be reported elsewhere. The overall coefficient of variation of the target volumes was approximately 17%, and the inter-institutional variations in target delineation were acceptable.

Phantom dosimetry test was also performed before starting the JCOG 0403 study to evaluate the accuracy of dosimetry in participating institutions to minimize inter-institutional variations. A lung phantom for SBRT was developed and used for this purpose. The absolute doses at the center of a simulated spherical tumor with a diameter of 3 cm in the lung were measured and compared with the calculated doses on-site by the responsible physicist.[12] The use of heterogeneity correction and different calculation algorithms both significantly influenced the accuracy of the absolute dose. The differences between the calculated doses with heterogeneity correction and measured doses were 4% for the Clarkson integration algorithm and 1% for the convolution-superposition algorithm. However, the Clarkson integration algorithm was selected for the JCOG 0403 study because the convolution-superposition algorithm was not available in some participating institutions at the beginning of this study.

CURRENT STATUS AND FUTURE DIRECTIONS

As of January 12, 2007, 111 patients were enrolled in this study. The accrual of operative patients has been completed, and that of inoperable patients will be completed in 2008. The final results for operable patients will be available in 3 years. At that time, we will be able to decide whether a randomized trial comparing SBRT to surgery is warranted or whether SBRT should be regarded as an alternative option for patients who refuse standard surgery. We also expect that CT criteria will be established to define local control by analyzing the serial CT data sets mandated in this study, because the response evaluation criteria in solid tumors (RECIST) are difficult to apply to see whether the tumor is eradicated because of secondary changes such as radiation fibrosis.

Another concern is the optimal dose schedule for this patient population. We selected 48 Gy in four fractions over 4 to 8 days based on retrospective data using BED formula; however, it has not been validated to be used in hypofractionated SBRT with a larger dose per fraction. Without a dose-finding phase I study, it is also hypothetical that 48 Gy in four fractions is enough to eradicate the tumor.

In the United States, prospective phase I and phase II studies have been performed at Indiana University.[13,14] Based on the results, they selected 60 Gy in three fractions over 1.5 to 2 weeks in the following RTOG trial, a phase II trial of SBRT in patients with medically inoperable stage I/II NSCLC (RTOG 0236). Not only is the dose schedule different from the Japanese schedule, but the target delineation, margins around the PTV, dose prescription (60% to 90%

isodose line vs. isocenter), and use of heterogeneity correction (uncorrected vs. corrected) are also different. These differences make it difficult to compare the results between these studies. Recently, the RTOG and JCOG have both decided to use an up-to-date and more accurate convolution-superposition algorithm with heterogeneity correction in the coming studies. The JCOG is now developing a dose-escalating phase I study for T2N0M0 NSCLC, and the RTOG is also developing a phase II study for operable patients with stage I NSCLC. We hope that these studies will define the optimal dose schedule and lead to standardization of the SBRT technique. Furthermore, international collaboration will be critical to establish the role of SBRT in the treatment of lung cancer.

REFERENCES

1. The editorial board of the cancer statistics in Japan. Cancer statistics in Japan 2005. Foundation for promotion of cancer research. Available at http://www.ncc.go.jp/jp/statistics/2005/data03.pdf. Accessed May 24, 2007.
2. Uematsu M, Shioda A, Suda A, et al. Computed tomography-guided frameless stereotactic radiotherapy for stage I non-small cell lung cancer: a 5-year experience. *Int J Radiat Oncol Biol Phys* 2001;51:666–670.
3. Fukumoto S, Shirato H, Shimzu S, et al. Small-volume image-guided radiotherapy using hypofractionated, coplanar, and noncoplanar multiple fields for patients with inoperable Stage I nonsmall cell lung carcinomas. *Cancer* 2002;95:1546–1553.
4. Nagata Y, Negoro Y, Aoki T, et al. Clinical outcomes of 3D conformal hypofractionated single high-dose radiotherapy for one or two lung tumors using a stereotactic body frame. *Int J Radiat Oncol Biol Phys* 2002;52:1041–1046.
5. Wulf J, Haedinger U, Oppitz U, et al. Stereotactic radiotherapy for primary lung cancer and pulmonary metastases: a noninvasive treatment approach in medically inoperable patients. *Int J Radiat Oncol Biol Phys* 2004;60:186–196.
6. Zimmermann FB, Geinitz H, Schill S, et al. Stereotactic hypofractionated radiation therapy for stage I non-small cell lung cancer. *Lung Cancer* 2005;48:107–114.
7. Beitler JJ, Badine EA, El-Sayah, et al. Stereotactic body radiation therapy for nonmetastatic lung cancer: an analysis of 75 patients treated over 5 years. *Int J Radiat Oncol Biol Phys* 2006;65:100–106.
8. Nyman J, Johansson KA, Hulten U. Stereotactic hypofractionated radiotherapy for stage I non-small cell lung cancer–mature results for medically inoperable patients. *Lung Cancer* 2006;51:97–103.
9. Onishi H, Araki T, Shirato H, et al. Stereotactic hypofractionated high-dose irradiation for stage I nonsmall cell lung carcinoma: clinical outcomes in 245 subjects in a Japanese multiinstitutional study. *Cancer* 2004;101:1623–1631.
10. Ishikura S, Teshima T, Ikeda H, et al on behalf of the Japan Clinical Oncology Group. Initial experience of quality assurance in radiotherapy within the Japan Clinical Oncology Group (JCOG). *Radiother Oncol* 2002;64:S224.
11. Atagi S, Kawahara M, Tamura T, et al. Standard thoracic radiotherapy with or without concurrent daily low-dose carboplatin in elderly patients with locally advanced non-small cell lung cancer: a phase III trial of the Japan Clinical Oncology Group (JCOG9812). *Jpn J Clin Oncol* 2005; 35:195–201.
12. Nishio T, Kunieda E, Shirato H, et al. Dosimetric verification in participating institutions in a stereotactic body radiotherapy trial for stage I non-small cell lung cancer: Japan Clinical Oncology Group trial (JCOG0403). *Phys Med Biol* 2006;51:5409–5417.
13. McGarry RC, Papiez L, Williams M, et al. Stereotactic body radiation therapy of early-stage non-small-cell lung carcinoma: phase I study. *Int J Radiat Oncol Biol Phys* 2005;63:1010–1015.
14. Timmerman R, McGarry R, Papiez L, et al. Initial report of a prospective phase II trial of stereotactic body radiation therapy for patients with medically inoperable stage I non-small cell lung cancer. *Int J Radiat Oncol Biol Phys* 2005;63:S99.

Development of an ultrasmall *C*-band linear accelerator guide for a four-dimensional image-guided radiotherapy system with a gimbaled x-ray head

Yuichiro Kamino[a)]
Medical Systems Administration Office, Mitsubishi Heavy Industries, Ltd., 10, Oye-cho-Minato-ku, Nagoya, Aichi 455-8515 Japan

Sadao Miura
Medical Systems Administration Office, Mitsubishi Heavy Industries, Ltd., 2-16-5, Konan Minato-ku, Tokyo 108-8215 Japan

Masaki Kokubo
Advanced Therapeutic Development Department, Institute of Biomedical Research and Innovation, 2-2 Minatojima Minamimachi Chuo-ku, Kobe Hyogo 650-0047 Japan

Ichiro Yamashita and Etsuro Hirai
Medical Systems Administration Office, Mitsubishi Heavy Industries, Ltd., 2-16-5, Konan Minato-ku, Tokyo 108-8215 Japan

Masahiro Hiraoka
Department of Radiation Oncology and Image-applied Therapy, Kyoto University Graduate School of Medicine, 54 Shogoin Kawahara-cho, Sakyo-ku, Kyoto 606-8507 Japan

Junzo Ishikawa
Department of Electronic Science and Engineering, Kyoto University, Kyoto Daigaku Katsura, Nishikyo-ku, Kyoto 615-8510 Japan

(Received 7 October 2006; revised 4 March 2007; accepted for publication 5 March 2007; published 26 April 2007)

We are developing a four-dimensional image-guided radiotherapy system with a gimbaled x-ray head. It is capable of pursuing irradiation and delivering irradiation precisely with the help of an agile moving x-ray head on the gimbals. Requirements for the accelerator guide were established, system design was developed, and detailed design was conducted. An accelerator guide was manufactured and basic beam performance and leakage radiation from the accelerator guide were evaluated at a low pulse repetition rate. The accelerator guide including the electron gun is 38 cm long and weighs about 10 kg. The length of the accelerating structure is 24.4 cm. The accelerating structure is a standing wave type and is composed of the axial-coupled injector section and the side-coupled acceleration cavity section. The injector section is composed of one prebuncher cavity, one buncher cavity, one side-coupled half cavity, and two axial coupling cavities. The acceleration cavity section is composed of eight side-coupled nose reentrant cavities and eight coupling cavities. The electron gun is a diode-type gun with a cerium hexaboride (CeB_6) direct heating cathode. The accelerator guide can be operated without any magnetic focusing device. Output beam current was 75 mA with a transmission efficiency of 58%, and the average energy was 5.24 MeV. Beam energy was distributed from 4.95 to 5.6 MeV. The beam profile, measured 88 mm from the beam output hole on the axis of the accelerator guide, was 0.7 mm × 0.9 mm full width at half maximum (FWHM) width. The beam loading line was 5.925 (MeV) − I_b (mA) × 0.00808 (MeV/mA), where I_b is output beam current. The maximum radiation leakage of the accelerator guide at 100 cm from the axis of the accelerator guide was calculated as 0.33 cGy/min at the rated x-ray output of 500 cGy/min from the measured value. This leakage requires no radiation shielding for the accelerator guide itself per IEC 60601-2-1. © *2007 American Association of Physicists in Medicine.* [DOI: 10.1118/1.2723878]

Key words: *C*-band, linear accelerator, image-guided radiotherapy, gimbaled x-ray head

I. INTRODUCTION

We are developing a new four-dimensional image-guided radiotherapy system.[1] The system has an x-ray head composed of an ultrasmall linear accelerator guide and a multi-leaf collimator (MLC) on the gimbals mechanism as shown in Fig. 1.

The gimbals mechanism is supported on an O-Ring structure. As shown in Fig. 2, the O-ring structure provides isocentric motion for portal selection. Pan and tilt motions of the gimbals provide active compensation for the mechanical distortion of the O-ring to attain beam positioning with a predicted accuracy of ±0.1 mm and quick pursuit beam mo-

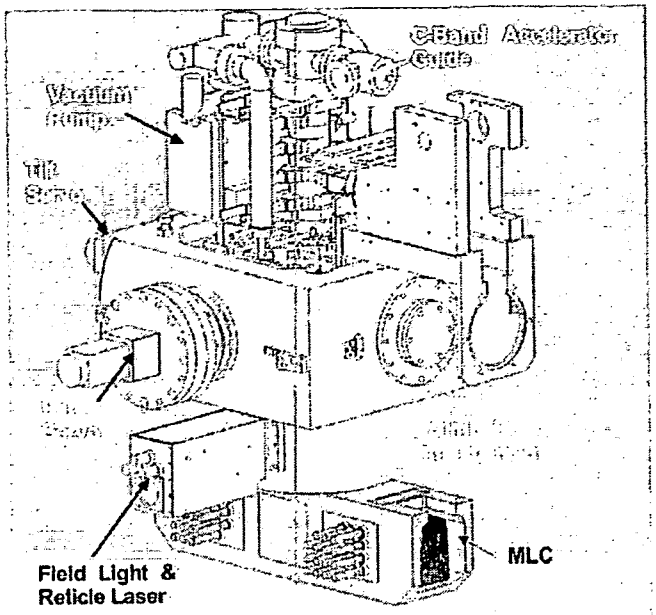

FIG. 1. The gimbaled x-ray head is composed of a *C*-Band accelerator guide, multi-leaf collimator, and gimbals mechanism.

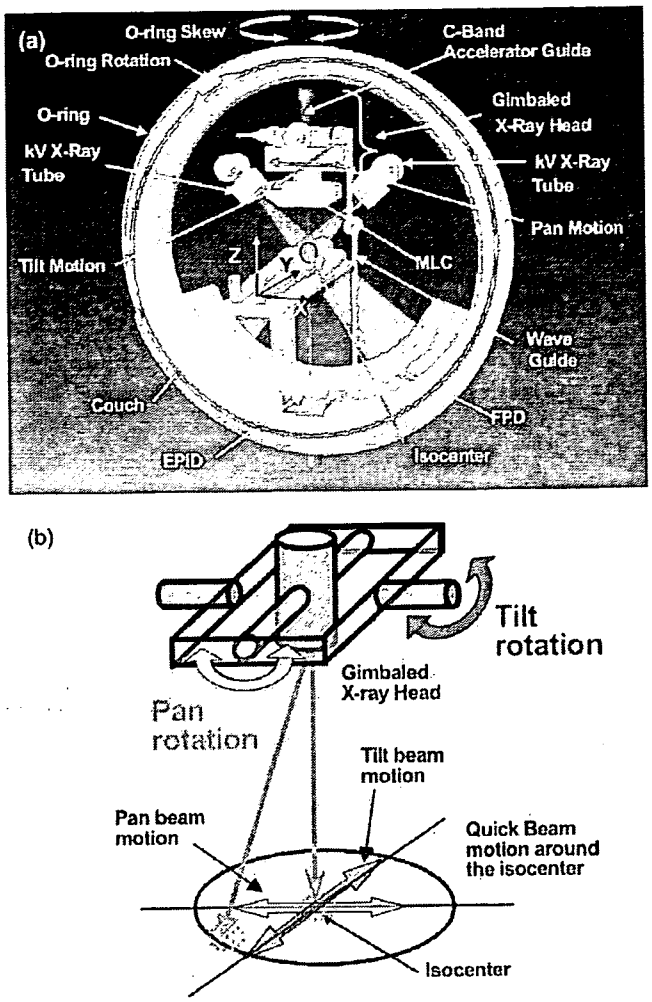

FIG. 2. The gimbaled x-ray head is mounted on the O-ring with 2 kV x-ray tubes and two flat panel detectors. The O-ring rotation provides portal selection around the isocenter and the O-ring skew provides the noncoplanar beam angles around the isocenter. The pan and tilt motions of the gimbals provide active compensation for the mechanical distortion and quick beam motion to compensate for the movement of the target around the isocenter.

tions to compensate for respiratory and cardiac movements. Because the frequency of the pan and tilt motions should be higher than 2 Hz to compensate for cardiac motion, the natural frequency of the gimbals and the support structure should be higher than 40 Hz to enable feedback control of the gimbals. The O-ring structure is necessary to attain the rigidity required for the gimbals motion, which the cantilever structure of a conventional medical electron linear accelerator cannot provide.

The history of the medical electron linear accelerator, including the history of the accelerator guide, is summarized concisely by Karzmark, Nunan, and Tanabe.[2] The weight and length of the accelerator guide and heavy and bulky ancillary devices such as x-ray shielding and magnetic focusing devices have been a problem, because an x-ray head composed of these devices must be movable around the patient. The majority of modern medical linear accelerators are isocentric machines, in which the gantry rotates around the isocentric axis. Most of the existing isocentric machines have cantilevered gantries to support x-ray heads. The gantry sags when rotated and the beam positioning accuracy is affected.[3,4] A huge counter mass is also required to stabilize the gantry.

Linear accelerator technology was developed for the *S* band (2.8–3 GHz) and was based on the *S*-band klystrons developed for military early warning radars. This technology carried over into the medical field, where today most conventional medical linear accelerators use this frequency band. The length of the accelerator guide depends on the energy of the beam and whether the accelerating structure is a traveling wave type or a standing wave type. A standing wave-type accelerator guide is shorter than a traveling wave type. The length of the standing wave-type accelerator guide is from 33 cm for 6 MV to 220 cm for 24 MV beams. The accelerator diameter, without side-coupling cavities, is about 10 cm. X-ray shielding is required around the accelerator guide to shield radiation leakage generated by beam loss in the guide. A small accelerator guide including x-ray shielding for a 6 MV beam weighs hundreds of kilograms. Mishin[5] presented a 6 MeV *X*-band (9.4 GHz) linear accelerator guide used for the CyberKnife®.[6] Though the diameter of the accelerator guide is about 3 cm and the weight is about 20 kg, the length of the accelerating structure is 58 cm and the total length of the accelerator guide including an electron gun is estimated to be about 65 cm.

Our system requires a new design approach. Because our system requires quick pan and tilt motions of the x-ray head on gimbals, in addition to the conventional isocentric rotation of the O-ring, the restrictions on weight and length of the x-ray head and the accelerator guide are much severer than for any other system. No existing accelerator guide for a medical linear accelerator is suitable for our system because

of its weight and size. The development of an ultrasmall and light accelerator guide was required to enable our concept.

II. METHODS AND MATERIALS

A. Establishment of the requirements for the accelerator guide

1. Electron beam energy

The preferred photon beam energy for treatment of brain, head and neck is 6 MV. This energy is also preferred for treatment of the thorax.[7,8] Treatment of deep-seated organs like the prostate or pancreas is possible with a 6 MV photon beam, if intensity modulation radiotherapy (IMRT) is used and more than nine nonopposed fields are assumed,[9,10] although a higher energy photon beam is preferable. If the electron beam energy is less than 6 MeV, there is a very low probability of neutron generation, and radiation shielding is much easier for a small and light x-ray head.[11] Based on these points, the requirement for the electron beam energy was set to 5–6 MeV.

2. Dose rate

Reduction of the time required for each dose fraction is important for efficient treatment and for the patient's comfort, especially for stereotactic radiotherapy or stereotactic radio surgery that requires more than 10 Gy per fraction. We set a requirement for the dose rate as 500 cGy/min in a monitor unit over a 15 cm × 15 cm maximum flattened field,[1] which is necessary for treatment of the prostate and neighboring lymph nodes.

3. Short settling time of beam energy spectrum

Because the delivered dose is controlled with a transmission ionization chamber in the x-ray head, fluctuation of the energy spectrum leads to fluctuation of the dose delivered to the target. In step and shoot IMRT, which requires frequent beam on and off, a short settling time of the energy spectrum is especially important.[12] The settling time performance is evaluated in terms of the small-dose accuracy defined by the dose error for a small dose at an appropriate point in a water phantom, but this performance includes various system errors and delays such as the delay and error of the transmission ionization chamber and the delay of the dose control circuit.

4. Minimization of penumbra

In IMRT, stereotactic radio-surgery, or stereotactic radiotherapy, it is important to give the prescribed dose to the prescribed area precisely and minimize the dose in other areas. The falloff characteristic of the fringe of the x-ray field is called the penumbra and is defined by the distance from the 80% dose area to the 20% dose area.[13] It is essential to reduce the spot size of the electron beam on the target to reduce the penumbra, although the penumbra is also affected by the cutoff and scattering characteristics of the collimators including the MLC. The spot size of the electron beam should be the minimum size acceptable to the x-ray target with respect to temperature and thermal stress.

5. Requirements on the mechanical property

The accelerator guide is installed in-line with the photon beam, because a bending magnet, which increases the weight unacceptably, is not allowed for the x-ray head. The x-ray head is installed on the structurally rigid O-ring to attain the mechanical response for the organ motion compensation. The source axis distance must be 100 cm to attain the same amount of clearance between the x-ray head and the patient as that of conventional medical linear accelerators. The diameter of the O-ring is governed by the length of the accelerator guide, and it is important to reduce the length of the accelerator guide to allow the O-ring to fit in an ordinary bunker.

The weight of the x-ray head should be minimized to attain the mechanical response needed for organ motion compensation.[1] The weight of the accelerator guide should be minimized. The accelerator guide and the beam line should not have any magnetic focusing device because of the weight and space limitations.

Leakage radiation shielding is another heavy item and should be minimized. The radiation shielding around the x-ray target is necessary to provide a required dose rate, but radiation shielding around the accelerator guide can be minimized by reducing beam loss in the high beam energy section of the accelerator guide.

The accelerator guide is installed on the gimbaled x-ray head and is subject to rotational motions for organ motion compensation. The accelerator guide, including the microwave feed line and vacuum pump, should be mechanically robust.

B. System design of the accelerator guide

1. Frequency band selection

A practical frequency range for a linear accelerator is the *L* band (1 GHz) to the *X* band (12 GHz). Theoretically, an accelerator guide could be designed and manufactured for any frequency in this range. However, availability of high peak power microwave sources limits the frequency selection. In the *S* band, many high peak power klystrons are available. High peak power magnetrons have also been developed for this frequency band and have been used for a high peak power microwave source. Above the *S* band, we have high peak power microwave sources initially developed for military tracking radars in the *C* band (5–6 GHz) and the *X* band (8–12 GHz). In the *C* band, Shintake and Matsumoto[14] have developed klystrons for scientific linear accelerator application in collaboration with Toshiba Co. Ltd. (1-1, Shibaura 1 chome, Minato-ku, Tokyo, Japan). And klystrons with peak power from 3 to 50 MW are commercially available. In the *X* band, a type of magnetron is commercially available for linear accelerator application,[5,6] but a klystron is still in the development phase.

The ease of production is an important consideration for an industrial product. The tolerance for an *X*-band accelera-

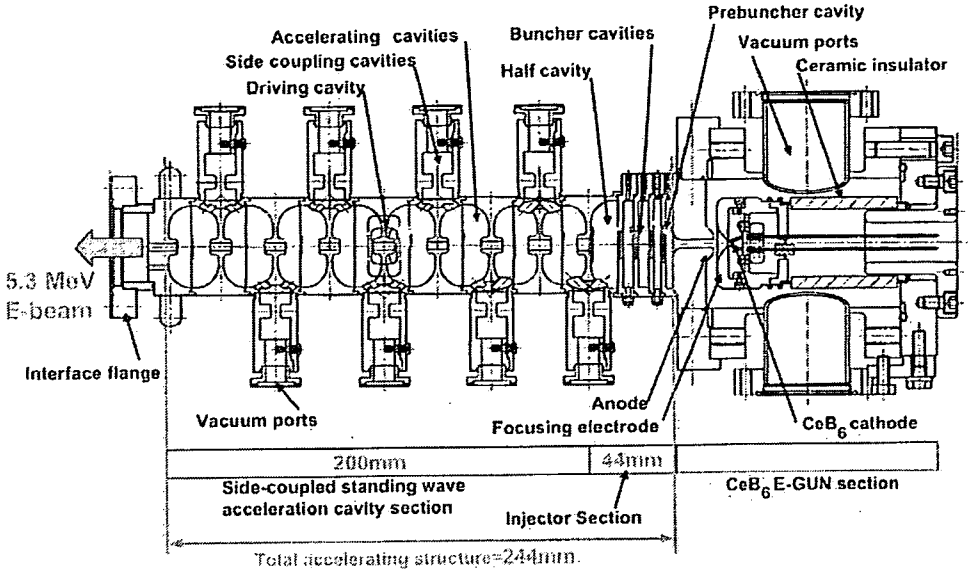

FIG. 3. The accelerator guide is composed of the electron gun section with a CeB_6 cathode, an injector section, and a side-coupled standing wave acceleration cavity section.

tor guide is one quarter of that for an *S*-band accelerator guide, and that for a *C*-band accelerator guide is one half of that for an *S*-band accelerator guide, if the structures are the same. Our experience shows that a *C*-band accelerator guide can be manufactured with the same manufacturing technology used for *S*-band accelerator guides, but an *X*-band accelerator guide requires some development in manufacturing technology. We chose the *C*-band with a frequency of 5.7 GHz as the best mix of size, weight, availability of the high peak-power microwave source, and production ease.

2. Output beam energy and beam current

As described in Sec. II A 1, all the beam energy was designed to be contained in the 4.8–5.9 MeV range, and the average beam energy was designed to be 5.3 MeV. Assuming a tungsten plate as an x-ray target, the optimum thickness was 1.45 mm as determined with EDMULT code.[15,16] The position and the shape of the aluminum flattening filter was also optimized with MCNP code[17] to provide a flattened x-ray field over a 15 cm × 15 cm field at the isocenter 100 cm from the x-ray target in 10-cm-deep water with a 20 cm water layer behind. The required average beam current was 55 μA. As common values were adopted for the beam pulse width and the repetition frequency as 3 μs and 300 Hz, the required beam current was 60 mA. With some margin, the beam current was designed to be 75 mA.

3. Beam loading

The settling characteristics of the beam energy at the beam-on are mainly determined by the drift of the resonant frequency of the accelerator guide due to thermal expansion caused by the ohmic loss of microwave power in the accelerating structure. The start-up characteristics of the current from the electron gun are also an important factor. The drift of the resonant frequency of the accelerator guide has a time constant of about 30 s and can be compensated by an adequate automatic frequency control circuit.

The diode electron gun has a start-up transient, if the cathode is heated up by electron back bombardment, in which electrons slip off the phase of the accelerating field in the injector section and are reflected back against the cathode voltage to hit the cathode. The time constant is several seconds with the small cathode described in Sec. II D 1, but this time constant does not satisfy the requirement in Sec. II A 3. The gradient of the beam loading line should be gradual to minimize the variation of the electron beam energy against the variation of the beam current from the electron gun.

4. Beam optics

An intensive finite-element study of temperature history and thermal stress of the tungsten x-ray target showed that a 1-mm-diameter (1σ) was acceptable with some margin for 6 MeV, 75 mA, 3 μs, and 300 Hz beam pulses. The beam diameter on the x-ray target 7.7 cm from the output beam hole was about 1 mm (1σ).

C. Overall structure of the accelerator guide

A standing wave-type accelerator guide was adopted, because a high accelerating gradient can be expected in the low beam current region. The overall structure is shown in Fig. 3. The accelerator guide is composed of the electron gun section in which electrons are generated, the injector section in which the electrons are bunched, and the acceleration cavity section in which the bunched electrons are accelerated to the designed beam energy.

D. Detailed design of the accelerator guide

1. Detailed design of the electron gun

The cathode voltage was selected as 25 kV, to be supplied from the stationary frame via a flexible high-voltage insulated cable to the moving gimbaled x-ray head, even though a higher voltage is better from the viewpoint of beam focus-

ing because it suppresses the space charge effect and improves electron capture characteristics of the injector section.[18]

Because the expected transmission efficiency, which is defined as the ratio of the output beam current from the accelerator guide to the beam current of the electron gun, is about 50%, the rated output beam current is 150 mA. The maximum output beam current was designed to be 300 mA with a margin.

The optical characteristics of the electron gun were designed to provide laminar flow with a 150 mA beam current with a diameter of about 1 mm (1σ) at the center of the prebuncher cavity located 7 mm from the electron gun output beam hole. In a conventional electron gun, the electron beam is generated on a rather large surface area cathode, focused to the required beam diameter with a focusing electrode, and injected into a solenoidal magnetic field in which a focused flow (Brillouin flow) is attained. The electrons at outer positions get radial momentum, and it is difficult with this design to get a focused flow without a solenoidal magnetic field. So we adopted a small diameter cathode and the compression ratio, which is defined as the ratio between the surface area of the cathode and the cut area of the focused beam, was minimized. An intensive study of the cathode diameter and the electrode geometry was conducted with E-GUN code[19] and the cathode diameter was set as 2 mm.

A diode-type electron gun was adopted, although a triode gun is often used in modern medical linear accelerators because of the ease of controlling the beam current with a grid electrode. But the grid electrode is usually a mesh of woven wires, and the diameter of the grid wire is so small that such a mesh is not mechanically practical for a cathode with a small diameter. A modulating anode electron gun can control the beam current easily, but the insulation design of the modulation anode is cumbersome and it is difficult to reduce the size of the electron gun. The modulating anode requires a high voltage pulse circuit (about 1 kV) at the floated cathode potential, which requires a complicated insulated anode modulation circuit.

An impregnated barium cathode is popular for the electron gun of modern medical linear accelerators. However, the practical emission current density is limited to 70 mA/mm^2 at the normal operation temperature; and an emission current density of 96 mA/mm^2 with a 2-mm-diam cathode, which is necessary for a 300 mA beam current, is not available. A cerium hexaboride (CeB_6) crystal cathode was selected. This cathode has a high emission current density of 200 mA/mm^2 at the normal operating temperature. The fringes of the electrodes were shaped to suppress the maximum surface electric field to less than 10 kV/mm for voltage-breakdown free and stable operation.

The CeB_6 cathode is a direct heating-type cathode and the heater current flows through the CeB_6 crystal. The magnetic field of the heater current will distort the trajectory of low energy electrons emitted from the surface of the CeB_6 crystal. So the heater current was designed to be a sinusoidal wave synchronized to the pulse repetition frequency. The cathode high voltage pulse is applied when the heater current crosses zero and the electrons are extracted when the magnetic field of the heater current is zero.

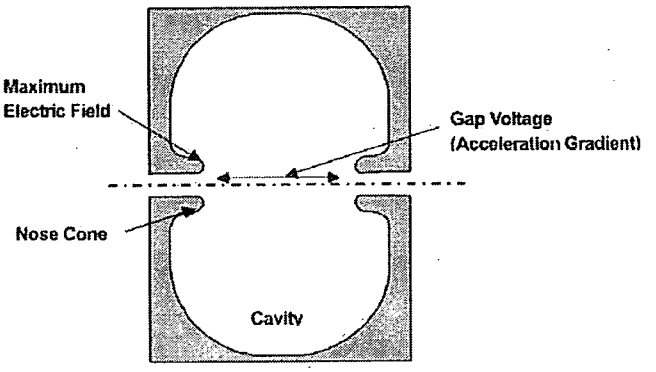

FIG. 4. The maximum electric field appears on the nose cone of the nose reentrant cavity. The ratio of maximum electric field to the acceleration gradient on the axis is 4.3.

2. Detailed design of the accelerating structure

The expected energy gain is 0.3 MeV for the injector section and 5.0 MeV for the acceleration cavity section.

a. Detailed design of the acceleration cavity section. The acceleration cavity section is composed of side-coupled nose reentrant cavities. Kilpatrick's criterion[20] specifies the vacuum breakdown voltage as 65 MV/m for 5.7 GHz. Tanabe[21] proposed 240 MV/m as the vacuum breakdown voltage based on experiments in which he observed the reflected microwave power from the nose reentrant half cavity with a 4.4 μs high peak power microwave of 2997 MHz. If Kilpatrick's relation between the frequency and the breakdown voltage can be applied to this number, the breakdown electric field is 340 MV/m for 5.7 GHz. However, Matsumoto[22] showed that field emission, with a local electric field enhanced by a microscopic geometry of the inner surface of the cavities, was the source of dark current even at voltages far below the breakdown voltage. The dark current is expected to have bad optical characteristics and seems to be a source of the leakage radiation from the accelerator guide. Inagaki *et al.*[23] measured dark current from a traveling wave-type *C*-band high gradient accelerator guide. His result shows that a non-negligible amount of dark current is expected at over 100 MV/m surface electric field strength. So we adopted 120 MV/m as a design criterion in the beam-loaded condition. The maximum surface electric field appears at the cavity-side tip of the nose cone of the cavity as determined from mathematical analysis with SUPERFISH code[24] (Fig. 4).

Because the ratio of the maximum surface field to the acceleration gradient is calculated as 4.3, the maximum acceleration gradient is 28 MV/m. The expected energy gain is 5.0 MeV, and the electron bunches are designed to be situated about 20° ahead of the crest of the acceleration field for phase stability of electron bunches. Therefore, the necessary length of the acceleration cavity section is about 19 cm. The required number of cavities is eight because the length for

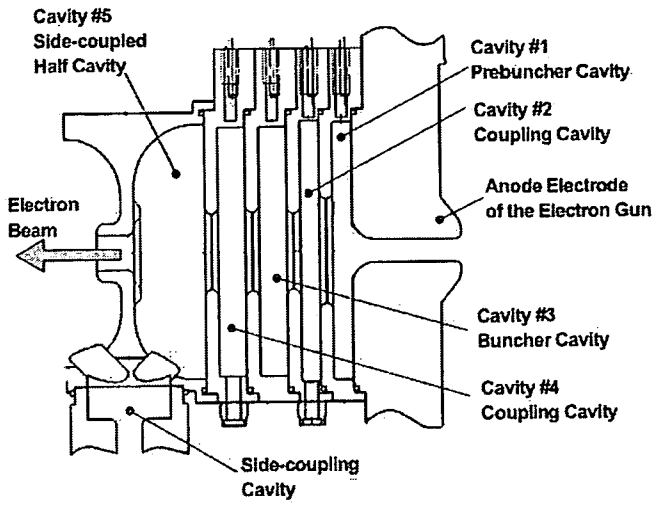

FIG. 5. The injector section is composed of five cavities. Cavity No. 1 is a prebuncher cavity. Cavity No. 3 and cavity No. 5 are buncher cavities. Cavity No. 2 and Cavity No. 4 are coupling cavities and do not contribute to acceleration. Cavity No. 1 through Cavity No. 4 are axial coupling cavities, which are coupled via beam holes. Cavity No. 5 is a side-coupled cavity and is fed from the acceleration cavity.

the $\pi/2$ mode cavity is 2.624 cm for 5712 MHz. The length of the low-energy side cavities was adjusted to accommodate electron bunches from the injector section with a speed less than that of light based on the beam dynamics simulation as shown in Sec. II D 2 d.

b. Detailed design of the injector section. Figure 5 shows the design of the injector section. A popular design of the injector for medical linear accelerators is to launch the electrons from the electron gun directly into a high acceleration gradient buncher cavity,[25] which is composed of a side-coupled half cavity and succeeding full cavities, but we provided a prebuncher cavity for our accelerator guide just after the electron gun to improve the bunching characteristics and minimize the beam loss in the acceleration cavity section.

Because the acceleration gradient of the prebuncher is much lower than that of the succeeding buncher cavities, the prebuncher cavity is usually driven independently from an external microwave source divided from the main feed line through an attenuator and a phase shifter. But these devices are too large and heavy to be installed on the gimbals mechanism, and the feed line will give phase variations that lead to variation of the beam energy and optics if it is mechanically bent by pan and tilt rotations. Therefore, an internal coupling to the prebuncher was included in the acceleration structure itself.

The prebuncher and succeeding buncher cavities are $\pi/2$ mode axial-coupled cavities. The cavity length must be reduced to synchronize the phase velocity of the accelerating microwave to the slow electron from the electron gun. The side-coupled cavity was avoided, because it is not practical to produce. Axial coupling is also better for the beam optics. The side-coupled cavity has a slight asymmetry of the radial electric field caused by the asymmetric side-coupled structure, and the asymmetry of the electric field will give an optical distortion to the low energy beam.

The prebuncher cavity (cavity No. 1) is succeeded by the coupling cavity (cavity No. 2). Cavity No. 2 does not contribute to the acceleration but works as a drift space before the buncher cavity (cavity No. 3). The buncher cavity is driven through the coupling cavity (cavity No. 4). The last cavity of the injector section is a side-coupled half cavity.

c. Beam loading effect. The accelerator guide is coupled to the external microwave circuit at the driving cavity through the coupling iris. Although the impedance-matched coupling coefficient β_0 is 1.4 for a beam current of 75 mA, β_0 was designed to be 1.6 (a slightly over-coupled condition). The beam loading curve is described with the following equation:

$$V=\frac{2\sqrt{\beta_0}}{1+\beta_0}\sqrt{P_{\mathrm{RF}}r\ell}\cos\phi-\frac{r\ell}{1+\beta_0}I_b, \tag{1}$$

where V is acceleration energy, P_{RF} is the input microwave power, ℓ is the length of the acceleration structure, ϕ is the phase ahead angle of the electron bunches from the crest of the acceleration electric field, I_b is the beam current, and r is the shunt impedance of the acceleration structure. The design values were P_{RF}=2.0 MW, ℓ=0.21 m, ϕ=20° ahead from the crest of the acceleration electric field, and I_b=75 mA. SUPERFISH code gives the calculated shunt impedance as 150 MΩ/m for the acceleration cavity, but the realistic value is empirically 90% of the calculated value because of imperfections of the machined surface. The injector section has a lower shunt impedance and the total shunt impedance of the whole acceleration structure is about 100 MΩ/m. These values were placed in Eq. (1) and, for a no-load energy (V at I_b=0) of 5.925 MeV, the slope of the beam loading curve is −0.00808 MeV/mA and the estimated beam energy at I_b =75 mA is 5.3 MeV.

d. Design optimization with mathematical simulation. SUPERFISH code was used for the design optimization of each cavity of the acceleration structure. MAFIA[26] code was used for the design optimization of the side-coupling structures and the coupling iris of the driving cavity. The gap voltage for each cavity was optimized in the beam dynamics simulation with EMSYS[27] code. EMSYS code is a field-charge-interaction code with particle-in-cavity simulation capability. PARMELA[28] code is usually used for the beam dynamics simulation of an electron linear accelerator. But PARMELA code requires manual input of gap voltage and the beam loading effect for each cavity. PARMELA code can not be applied to this accelerator guide, for which neither gap voltage nor beam loading effect can be determined explicitly, because the injector section with a complex structure is combined with the acceleration cavity section and is fed internally from the acceleration cavity section. However, EMSYS can give a self-consistent beam loading effect evaluation. E-GUN code gave an initial condition of the electron beam for EMSYS code. The optimization was an iterative process of the beam dynamics simulation with EMSYS code.

e. Thermal analysis. Thermal analysis of the cavity was performed with ANSYS[29] code with the heat input of the ohmic loss of the microwave current calculated with SUPER-

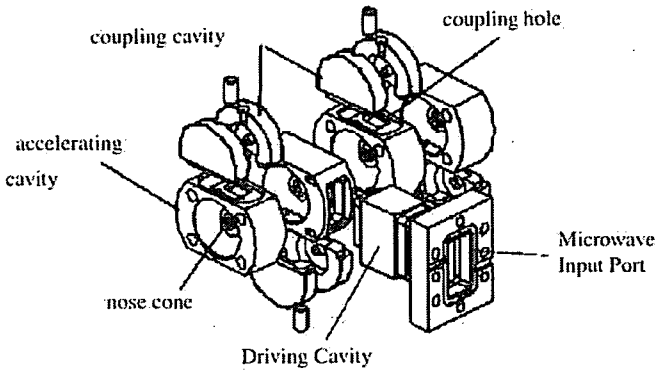

FIG. 6. The accelerating cavities and the coupling cavities have bipartite structure.

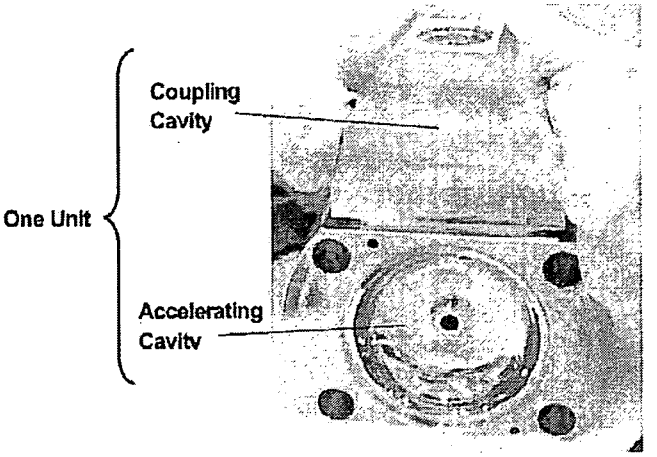

FIG. 8. One unit of the accelerating guide is composed of an accelerating cavity and a coupling cavity.

FISH code. The nose cone had the highest temperature of 51 °C when cooled with 30 °C water and no thermal problem was expected. The resonance frequency of the accelerator guide is shifted because of the thermal expansion, but a proper automatic frequency control mechanism can compensate for this effect.

E. Manufacturing the accelerator guide

The construction of the accelerating cavities and coupling cavities is shown in Fig. 6. The cavities of the accelerator guide are made of oxygen-free high conductivity copper (ASTM F68 Class1). The cavity parts are shown in Fig. 7. The inner surfaces of the accelerating cavities were finished with an ultraprecision lathe to reduce the risk of microwave discharge. Both the accelerating cavities and coupling cavities have bipartite structure. One set of coupling cavities was vacuum soldered to the two half-accelerating cavities and constituted one unit as shown in Fig. 8. These units were assembled and vacuum soldered to constitute the whole accelerator guide. The coupling hole between the accelerating cavity and the coupling cavity was machined with a milling machine. The axis of the coupling hole was inclined by 45° to the axis of the accelerator guide. With this design, a sharp edge was eliminated from the edge around the coupling hole and the risk of microwave discharge was reduced.

The parts of the electron gun were made of stainless steel (UNS S30403). The cathode assembly, which is composed of cathode and focusing electrode, was supported on a ceramic insulator cylinder. The focusing electrode was made of molybdenum to withstand the heat from the nearby CeB_6 cathode. The parts of the electron gun are shown in Fig. 9 with the CeB_6 cathode in the upper left of the figure. The anode electrode flange of the electron gun is the wall of the prebuncher cavity as shown in Fig. 5. The cathode assembly is

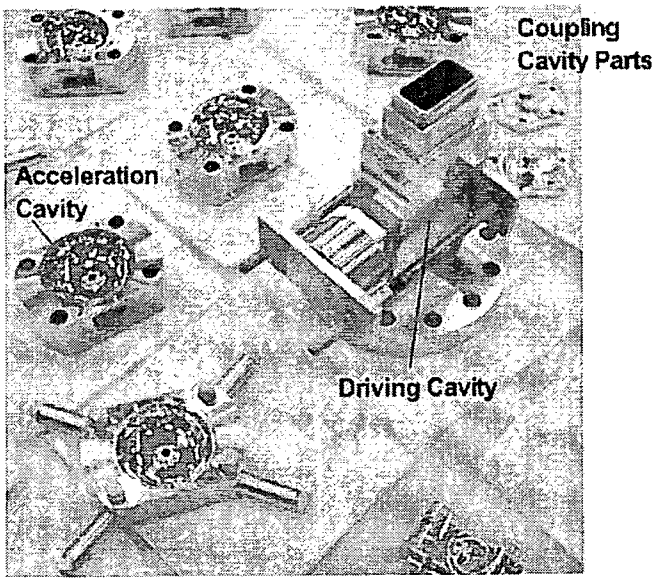

FIG. 7. The cavity parts are made of oxygen-free high conductivity copper (ASTM F68 Class 1) and the inner surfaces are machined with an ultraprecision lathe.

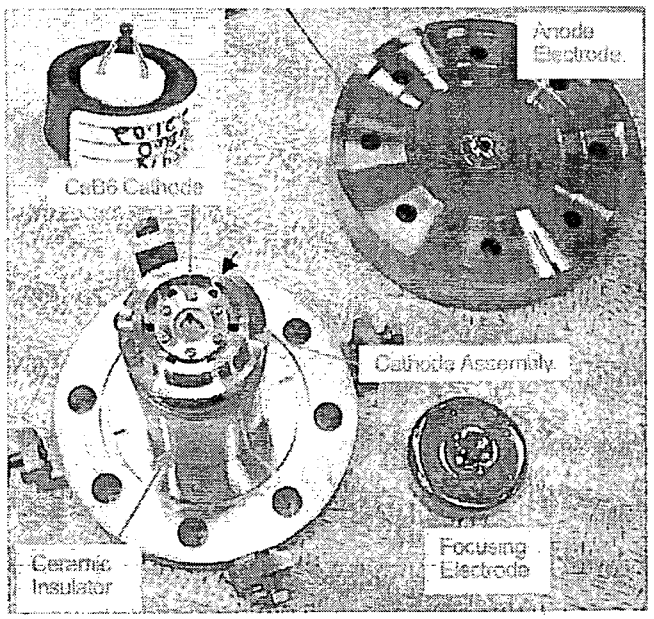

FIG. 9. The electron gun is composed of an anode electrode, cathode assembly, focusing electrode, and ceramic insulator.

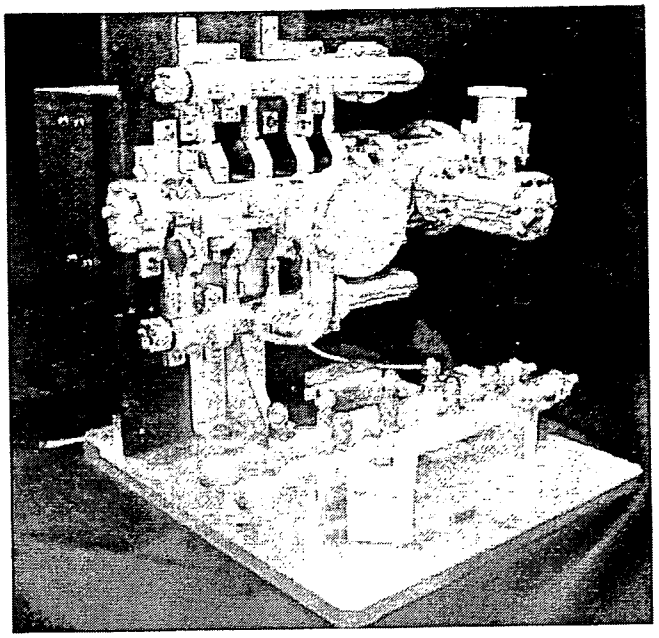

FIG. 10. The accelerator guide assembled on the test stand.

bolted to the anode flange via the vacuum vessel of the electron gun. The accelerator guide assembled on the test stand is shown in Fig. 10.

The prototype accelerator guide is 38 cm long and the weighs about 10 kg.

F. Evaluation of the accelerator guide

1. Evaluation of the electron gun

Before being attached to the accelerator guide, the beam profile of the electron gun was measured with a two-dimensional wire scanner. The cathode voltage and electron beam current were set to the designed values of −25 kV and 155 mA.

2. Evaluation of the whole accelerator guide

The beam characteristics of the accelerator guide were measured with the test bench shown in Fig. 11. Pulses of 5 μs were fed to the accelerator guide through a circulator and waveguides. The peak microwave power at the klystron output was 3.1 MW, and the microwave power was estimated to be 2.0 MW at the input of the accelerator guide. The frequency was adjusted to minimize the reflection power from the accelerator guide to get the tuned condition around the design frequency of 5712 MHz. The pulse repetition frequency was set to 10 Hz.

The transmission efficiency was calculated by dividing the reading of current monitor (CM) No.1 in Fig. 11 with the cathode current supplied to the electron gun.

A slit scanner with a slit thickness greater than the stopping range for a 6 MeV electron was used to measure the beam profile (the geometrical distribution of the beam current in the cut section of the beam). The slit width was 0.2 mm and the beam current through the slit was monitored with current monitor No. 1. The measurement was made in the plane perpendicular to the axis of the accelerator guide at a position 88 mm from the output beam hole of the accelerator guide, which is 11 mm farther than the designed x-ray target position because of the mechanical limitation of our experiment setup.

The energy distribution of the beam was measured with the 90° beam bending magnet as shown in Fig. 11. The radius of the central beam path in the bending magnet was 175 mm and the aperture of the energy analyzing slit was 4 mm, which corresponded to a resolution of 0.05 MeV. The measurement was conducted for output beam currents (I_b) of 50 and 75 mA (designed beam current), 100 and 125 mA with 2.0 MW of the estimated microwave power at the input of the accelerator guide. The measurement was also made for 1.64, 1.74, 2.0 and 2.1 MW of the estimated microwave input power with the output beam current of 75 mA.

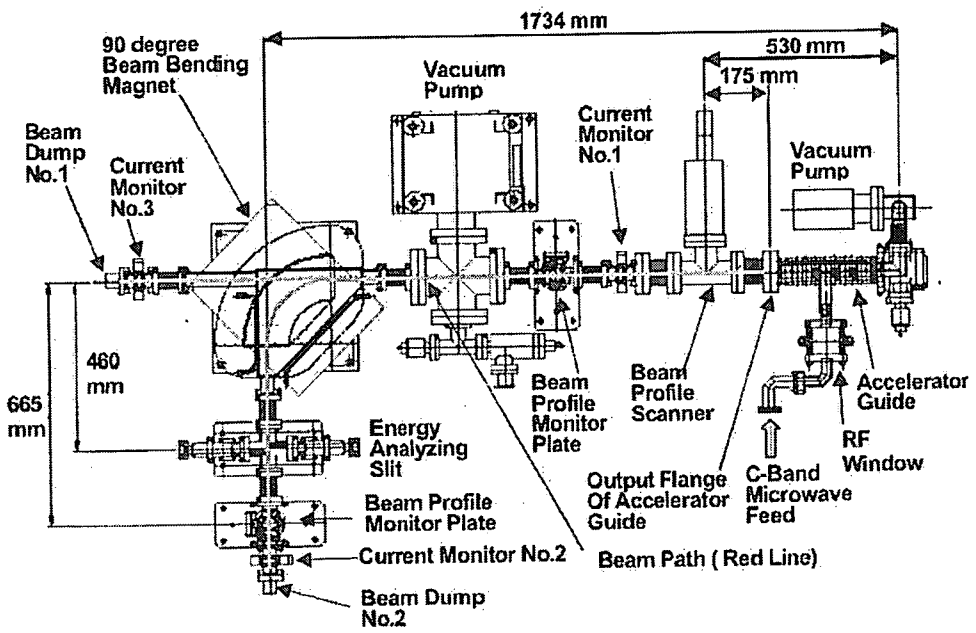

FIG. 11. Outline of the accelerator test bench. The beam profile scanner has slits movable in two axes on the plane perpendicular to the beam line. Current monitor No. 1 is used to measure the output beam current and the beam profile. The beam is magnetically analyzed with the 90° beam bending magnet. The beam energy distribution is measured with the energy analyzing slit and current monitor No. 2.

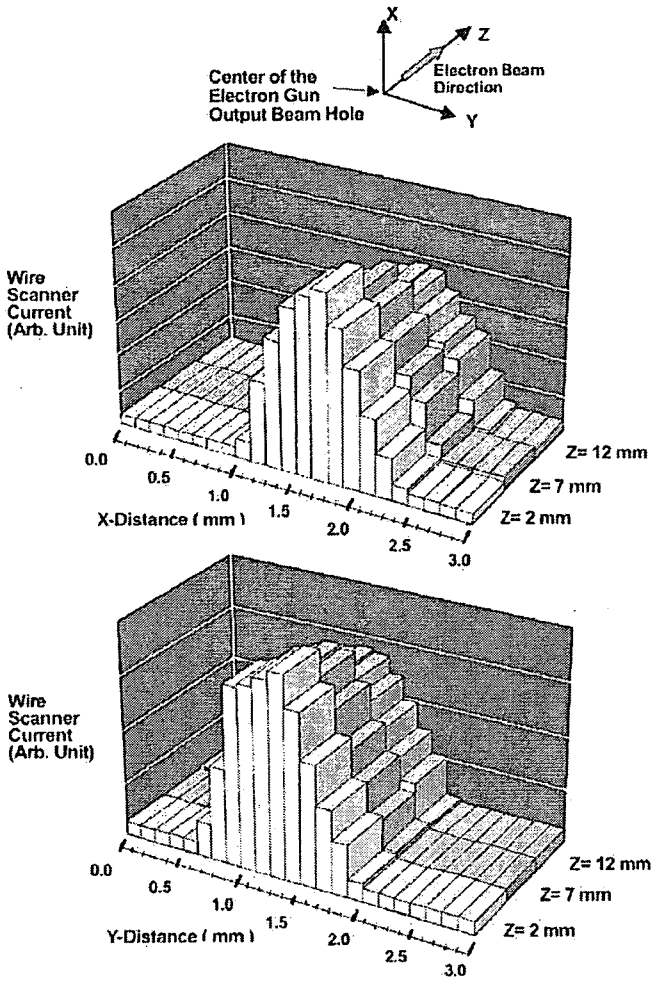

FIG. 12. Beam profile of the electron beam of the electron gun measured at −25 kV, 155 mA.

The leakage radiation was measured with a PTW Farmer ionization chamber, Model 30013 (PTW, Freiburg GMBH 79115, Lorracher Strasse 7, Freiburg Germany), equipped with a 6 MV buildup cap and a cylindrical lead collimator 15 cm long and 15 cm outer diameter, and a 5-cm-diam bore at the center. The ionization chamber was scanned along the axis of the accelerator guide at a distance of 35 cm from the axis of the accelerator guide, with the axis of the collimator perpendicular to the axis of the accelerator guide and in the looking-down direction in Fig. 11. The accelerated electron beam was dumped to beam dump No.1, which was shielded with lead bricks.

III. RESULTS AND DISCUSSION

A. Beam characteristics of the electron gun

The measured beam profile (Fig. 12) shows that laminar flow with full width at half maximum (FWHM) diameter of about 1 mm was attained from 2 to 12 mm from the output beam hole of the electron gun, which corresponds to the locations of Cavity No. 1 (Prebuncher cavity) through Cavity No. 3 (Buncher Cavity) in Fig. 5. If the normal distribution is assumed for the beam profile, the diameter for 1σ is 0.85 mm.

TABLE I. Transmission efficiency of the accelerator guide calculated by dividing the reading of current monitor No.1 in Fig. 11 by the cathode current supplied to the electron gun.

Output beam current (I_b) (current monitor No.1)	50 mA	75 mA	100 mA	125 mA
Electron gun current (I_c) (cathode current)	100 mA	130 mA	180 mA	285 mA
Transmission efficiency (I_b/I_c)	50%	58%	56%	44%

B. Beam characteristics of the whole accelerator guide

1. Beam current and transmission efficiency

The output beam current and transmission efficiency are listed in Table I. The transmission efficiency was more than 50% at the designed operating condition (output beam current of 75 mA). This value is much higher than that of about 30% with the majority of standing wave type accelerator guides[25] for existing *S*-band medical linear accelerators, in which the electron beam from the electron gun is launched directly into a high acceleration gradient half cavity. Higher transmission efficiency is beneficial for the design of the electron gun and the low energy part of the injector section because it relaxes the space charge effect.

2. Beam profile

The beam profile is shown in Fig. 13 for output beam current of 75 mA. The FWHM beam width was 0.9 mm on the *X* axis and 0.7 mm on the *Y* axis. This result corresponds to a 0.8 mm (*X* axis) by 0.6 mm (*Y* axis) (1σ) elliptical beam, if the normal distribution is assumed. The beam profile is a little bit sharper than designed.

The slight asymmetry in the beam profile seems to be the result of the axial asymmetry of the accelerating electric field within the accelerator guide, because the accelerating structure is geometrically asymmetric due to the side-coupled structure. Because the penumbra characteristics are affected by the design of the downstream components (x-ray target, flattening filter, and collimators including MLC), the penumbra should be evaluated as an integrated x-ray head.

3. Beam energy distribution

Figure 14 shows the beam energy distribution measured for various output beam currents (I_b) and Fig. 15 shows the energy distribution measured for various input microwave powers. In Fig. 14, the beam energy distribution has a single peak for I_b=100 mA and I_b=125 mA, but it has multiple peaks for I_b less than 75 mA. This phenomenon was understood as follows through the beam dynamics simulations with EMSYS.

In the bunching process in the injector section, a portion of electrons slips off from the electron bunch. When the ac-

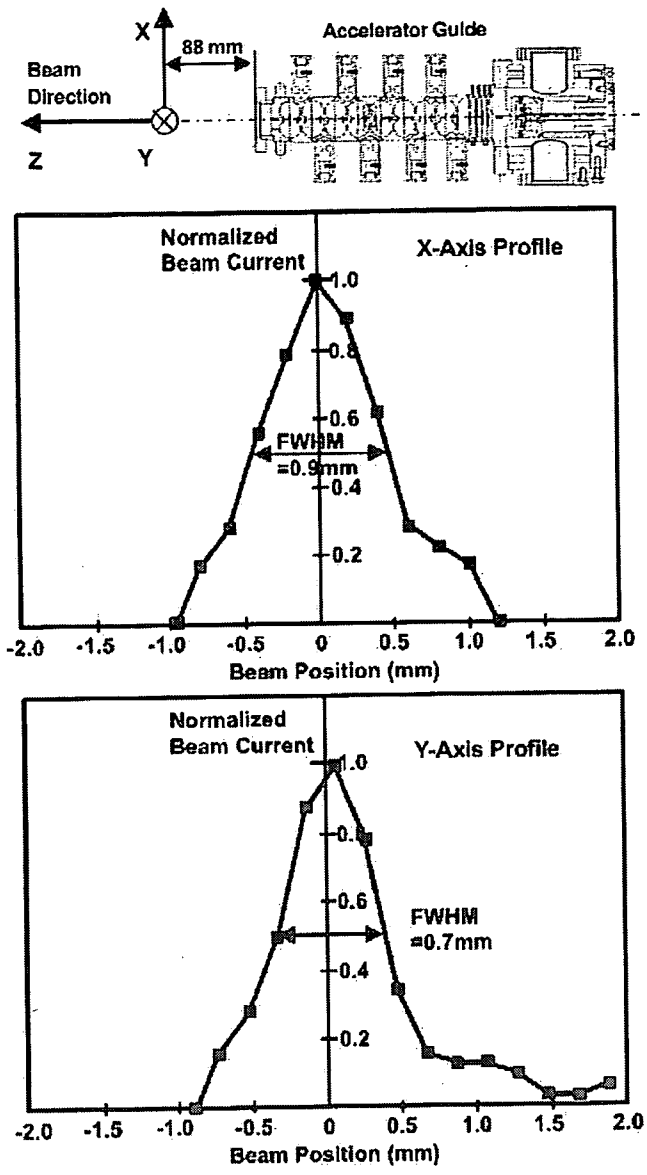

FIG. 13. Beam profile measured 88 mm from the output beam hole of the accelerator guide.

celeration gradient is high in the injector section, these electrons are captured in the succeeding electron bunch and constitute the second distribution in this bunch. This mechanism causes multiple peaks in the beam energy distribution. When I_b=50 mA, the beam loading is light and the acceleration gradient is high, which results in multiple peaks in the energy distribution. When I_b=100 mA or I_b=125 mA, the beam loading is heavy and the acceleration gradient is lower. The electrons slipping off from the bunch are not captured in the succeeding bunch and the energy profile has a single peak.

When the input microwave power is increased with a constant output beam current, the acceleration gradient is increased in the injector section and the same multiple peaks phenomenon is observed as shown in Fig. 15.

In addition to this phenomenon, the beam will be over focused when I_b<50 mA and will be under focused when

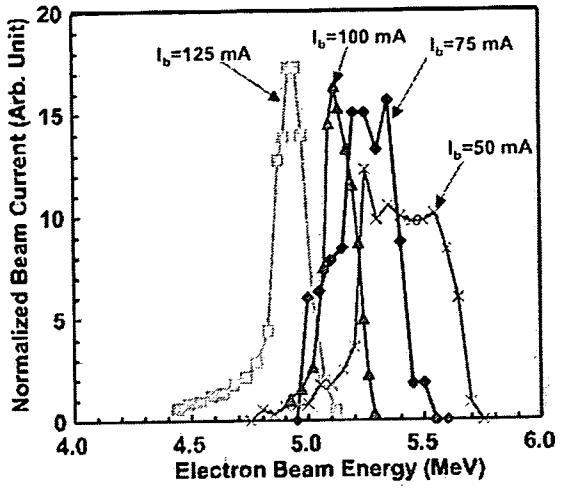

FIG. 14. Beam energy distribution measured for I_b=50, 75, 100, and 125 mA with a microwave input P_{RF}=2.0 MW. The normalized beam current is the percentage of the current in a 0.05 MeV window with respect to the total current.

I_b>125 mA, because the focusing in the electron gun and the injector section is optimized at I_b=75 mA to balance against the space charge effect. It will be necessary to operate this accelerator guide in a rather narrow range of I_b around the designed I_b of 75 mA.

4. Beam loading characteristics

The beam loading characteristics calculated from the result in Fig. 14 are shown in Fig. 16. The black dots correspond to each averaged energy distribution weighted with the corresponding beam current. The designed beam loading line presented in Sec. II D 2 c is shown in the figure. The average beam energy weighted with the beam current was 5.24 MeV for I_b=75 mA, which is in good agreement with the designed

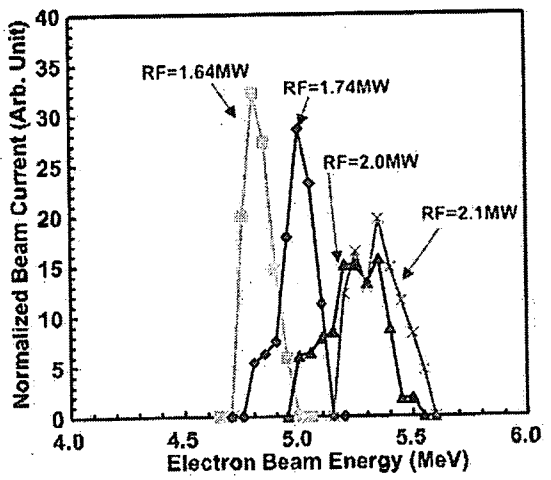

FIG. 15. Beam energy distribution measured for a microwave input P_{RF} =1.64, 1.74, 2.0, and 2.1 MW with I_b=75 mA. The normalized beam current is the percentage of the current in a 0.05 MeV window with respect to the total current.

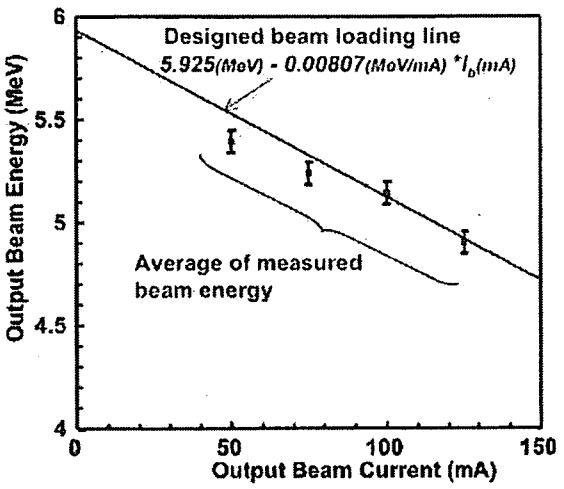

FIG. 16. Beam loading characteristics calculated from the beam energy distribution in Fig. 14. The theoretical beam loading line is also shown. Error bars show the measurement error caused by the resolution of the energy analyzing setup (i.e., the 90° bending magnet and the energy analyzing slit).

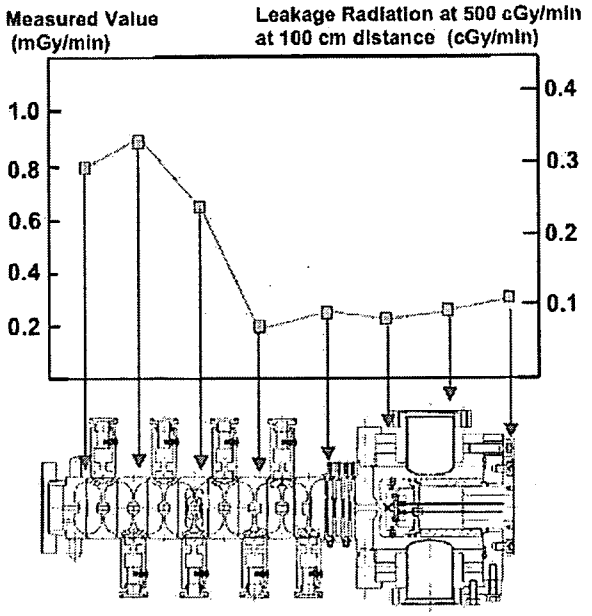

FIG. 17. Leakage radiation from the accelerator guide measured with a Farmer ionization chamber with a 15-cm-long lead collimator at 35 cm from the axis of the accelerator guide. The ionization chamber was scanned along the axis of the accelerator guide with the axis of the collimator perpendicular to the axis of the accelerator guide and in the looking-down direction in Fig. 11.

beam energy of 5.3 MeV. At I_b=75 mA, the beam energy was distributed between 4.95 and 5.6 MeV.

The low gradient of the beam loading line ensures the stability of the x-ray energy against the beam current variation. Figure 16 shows that ±10% fluctuation of the electron beam current causes ±0.06 MeV energy fluctuation. However, the small dose accuracy must be evaluated for the whole accelerator system and will be reported in another paper.

5. Leakage radiation from the accelerator guide

The measured result is shown in Fig. 17. The maximum leakage radiation was observed at the high-energy section of the accelerator guide, and the value was 0.9 mGy/min. From this value, the maximum leakage radiation at the rated x-ray output of 500 cGy/min (pulse repetition frequency of 300 Hz) and at 100 cm from the accelerator guide was calculated as 0.33 cGy/min and 0.066% of the rated x-ray output, which satisfies the IEC60601-2-1 (Ref. 30) requirement (less than 0.1% (average) and 0.2% (maximum) of the treatment beam) without any radiation shielding around the accelerator guide. If the x-ray target is set at the designed position of 77 mm from the output flange, backscattering is expected through the beam hole of the accelerator guide and radiation shielding will be necessary just behind the electron gun.

IV. CONCLUSION

An ultrasmall and light *C*-band linear accelerator guide was developed for our four-dimensional image-guided radiotherapy system. The accelerator guide is 38 cm long including the electron gun and weighs about 10 kg. The length of the accelerating structure is 24.4 cm. The accelerating structure is a $\pi/2$ mode standing wave type and is composed of an axial-coupled injector section and a side-coupled acceleration cavity section. The injector section is composed of one prebuncher cavity, one buncher cavity, one side-coupled half cavity and two axial coupling cavities. The acceleration cavity section is composed of eight side-coupled nose reentrant cavities and eight coupling cavities. The electron gun is a diode-type gun with a CeB_6 direct heating cathode. The accelerator guide can be operated without any magnetic focusing device.

The output beam current was 75 mA with a transmission efficiency of 58%. The average energy was 5.24 MeV. The beam energy was distributed from 4.95 to 5.6 MeV. The beam profile was 0.7 mm×0.9 mm FWHM width at the 88 mm point on the axis of the accelerator guide. The beam loading line was 5.925 (MeV)$-I_b$ (mA) ×0.00808 (MeV/mA).

The maximum leakage radiation of the accelerator guide at the rated x-ray output of 500 cGy/min was calculated as 0.33 cGy/min 100 cm from the accelerator guide. This leakage level requires no radiation shielding for the accelerator guide itself per IEC 60601-2-1.

ACKNOWLEDGMENTS

We are very thankful to Dr. Tsumoru Shintake of the RIKEN Harima Institute and Dr. Hiroshi Matsumoto of the Japanese National Organization for High Energy Accelerator Research (KEK). The technology for the *C*-band standing wave-type accelerator guide came from a joint research and development program with Dr. Shintake and Dr. Matsumoto conducted in 1998 and 1999. We depend a lot on them for other *C*-band accelerator technology including klystron and *C*-band devices. Related presentations were made at the 46th annual meeting of the American Association of Physicists in

Medicine (AAPM) (Pittsburgh, Pennsylvania, July 2004) by Kamino *et al.*; at the 46th annual meeting of the American Society for Therapeutic Radiology and Oncology (ASTRO) (Atlanta, Georgia, October 2004) by Takayama *et al.*; and at the 47th meeting of ASTRO (Denver, Colorado, October 2005) by Takayama *et al.*

[a]Electronic mail: yuichirokamino@nifty.com

[1]Y. Kamino, K. Takayama, M. Kokubo, Y. Narita, E. Hirai, N. Kawada, T. Mizowaki, Y. Nagata, T. Nishidai, and M. Hiraoka, "Development of a four-dimensional image-guided radiotherapy system with a gimbaled x-ray head," Int. J. Radiat. Oncol., Biol., Phys. **66**, 271–278 (2006).

[2]C. J. Karzmark, C. S. Nunan, and E. Tanabe, *Medical Electron Accelerators* (McGraw–Hill, New York, 1993).

[3]AAPM Report No. 54 "Stereotactic Radiosurgery," (1995).

[4]J. Rahimian, J. C. Chen, A. A. Rao, M. R. Girvigian, M. J. Miller, and H. E. Greathouse, "Geometrical accuracy of the Novalis stereotactic radiosurgery system for trigeminal neuralgia," J. Neurosurg. **101**Suppl. 3, 351–355 (2004).

[5]A. V. Mishin, "Advances in X-band and S-band linear accelerators for security, ND, and other applications," *Proceedings of 2005 Particle Accelerator Conference*, Knoxville, Tennessee, pp. 240–244 (2005).

[6]J. R. Adler, Jr., S. D. Chang, M. J. Murphy, J. Doty, P. Geis, and S. L. Hancock, "The Cyberknife: A frameless robotic system for radiosurgery," Stereotact. Funct. Neurosurg., **69**, 124–128 (1997).

[7]J. S. Laughlin, R. Mohan, and G. J. Kutcher, "Choice of optimum megavoltage for accelerators for photon beam treatment," Int. J. Radiat. Oncol., Biol., Phys. **12**, 1551–1557 (1986).

[8]H. Garrison, J. Anderson, J. S. Laughlin, and R. A. Harvey, "Comparison of dose distributions in patients treated with x-ray beams of widely different energies," Radiology **58**, 361–368 (1952).

[9]S. Söderström, A. Eklöf, and A. Brahme, "Aspects on the optimal photon beam energy for radiation therapy," Acta Oncol. **38**, 179–187 (1999).

[10]A. Pirzkall, M. P. Carol, B. Pickett, P. Xia, M. Roach III, and L. J. Verhey, "The effect of beam energy and number of fields on photon-based IMRT for deep-seated targets," Int. J. Radiat. Oncol., Biol., Phys. **53**, 434–442 (2002).

[11]Ministry of Education, Culture, Sports, Science and Technology of Japanese Government, "Guideline for handling of radiation generators dated Oct. 30th 1998."

[12]M. B. Sharpe, B. M. Miller, D. Yan, and J. W. Wong, "Monitor unit settings for intensity modulated beams delivered using a step and shoot approach," Med. Phys. **27**, 2719–2725 (2000).

[13]IEC 976, "Medical electrical equipment medical electron accelerators—functional performance characteristics," p. 55 (1989).

[14]T. Shintake, N. Akasaka, H. Matsumoto, Y. Ohkubo, and H. Yonezawa, "Development of C-band 50 MW Pulse Klystron for e+ e− Linear Collider," KEK Preprint 97–94 (1997).

[15]R. Ito and T. Tabata, "Semi-empirical code EDMULT for depth-dose distributions of electrons in multilayer slab absorbers: Revisions and applications," Radiation Center of Osaka Prefecture Technical Report No. 8, Radiation Center of Osaka, Osaka Japan (Nov. 1987).

[16]T. Tabata, P. Andreo, and K. Shinoda, "An algorithm for depth-dose curves of electrons fitted to Monte Carlo data," Radiat. Phys. Chem. **53**, 205–215 (1998).

[17]T. Goorley, J. Bull, F. B. Brown, T. E. Booth, G. Hughes, R. D. Mosteller, R. A. Forster, S. E. Post, R. E. Prael, E. C. Selcow, A. Sood, and J. E. Sweezy, "Release of MCNP5_RSICC_1.30," LA-UR-04-4519, Los Alamos National Laboratory (2004).

[18]P. Brunet and X. Buffet, "Injectors," in *Linear Accelerators*, edited by P. M. Lapostolle and A. L. Septier (North-Holland, Amsterdam, 1970), pp. 237–264.

[19]W. B. Herrmannsfeldt, "EGUN—An electron optics and gun design program," SLAC Report No. 331, Stanford University (1988).

[20]W. D. Kilpatrick, "Criterion for vacuum sparking designed to include both RF and DC," UCRL-2321, Lawrence Berkeley National Laboratory (1953).

[21]E. Tanabe, "Voltage breakdown in S-band linear accelerator cavities," IEEE Trans. Nucl. Sci. **NS-30**, 3551–3553 (1983).

[22]H. Matusmoto, "Dark currents," *Proceedings of the 18th International Linac Conference*, Geneva, Switzerland, pp. 626–630 (1996).

[23]T. Inagaki, K. Onoe, T. Shintake, H. Baba, X. Marechal, S. Takahashi, H. Matsumoto, and S. Miura, "High gradient test on the C-band choke-mode type accelerating structure," *Proceedings of the 2nd Annual Meeting of Particle Accelerator Society of Japan*, 343–345 Saga pref. Japan (2005).

[24]J. H. Billen and L. M. Young, "SUPERFISH/Poisson Group of Codes," LA-UR-96-1834, Los Alamos National Laboratory (2003).

[25]C. J. Karzmark, C. S. Nunan, and E. Tanabe, *Medical Electron Accelerators* (McGraw–Hill, New York, 1993), pp. 49–87.

[26]M. Bartsch, M. Dehler, M. Dohlus, A. Fischerauer, G. Fischerauer, P. Hahne, R. Klatt, F. Krawczyk, P. Schütt, B. Steffen, S. Wipf, T. Weiland, and M. Zhang, "MAFIA Release 3: The new version of the general purpose electromagnetic design code family," *Proceedings of the 2nd European Particle Accelerator Conference*, Nice, France, pp. 249–251 (1990).

[27]T. Shintake, "Recent status of FCI: PIC simulation of coupled-cavity structure," *Proceedings of the 18th International Linac Conference*, Geneva, Switzerland, pp. 181–183 (1996).

[28]L. M. Young, "PARMELA," LA-UR-96-1835, Los Alamos National Laboratory (1996 rev. 2004).

[29]http://www.ansys.com

[30]IEC60601-2-1, "Medical electrical equipment—Particular requirements for the safety of electron accelerators in the range of 1 MeV–50 MeV" (1998).

Development of a new concept automatic frequency controller for an ultrasmall C-band linear accelerator guide

Yuichiro Kamino[a)]
Medical Systems Administration Office, Mitsubishi Heavy Industries, Ltd., 10, Oye-cho Minato-ku, Nagoya, Aichi 455-8515, Japan

Kazuhiro Tsukuda
Medical Systems Administration Office, Mitsubishi Heavy Industries, Ltd., 2-16-5 Konan Minato-ku, Tokyo 108-8215, Japan

Masaki Kokubo
Department of Image-based Medicine, Division of Radiation Oncology, Institute of Biomedical Research and Innovation, 2-2, Minatojima-Minaminachi, Chuo-ku, Kobe 650-0047, Japan

Sadao Miura and Etsuro Hirai
Medical Systems Administration Office, Mitsubishi Heavy Industries, Ltd., 2-16-5 Konan Minato-ku, Tokyo 108-8215, Japan

Masahiro Hiraoka
Department of Radiation Oncology and Image-applied Therapy, Kyoto University Graduate School of Medicine, 54 Shogoin Kawahara-cho, Sakyo-ku, Kyoto 606-8507, Japan

Junzo Ishikawa
Department of Electronic Science and Engineering, Kyoto University, Kyoto Daigaku Katsura, Nishikyo-ku, Kyoto 615-8510, Japan

(Received 4 March 2007; revised 3 June 2007; accepted for publication 5 June 2007; published 17 July 2007)

We are developing a four-dimensional, image-guided radiotherapy system with a gimbaled x-ray head. The system has pursuing irradiation capability in addition to precise irradiation capability, owing to its agile x-ray head. The moving x-ray head requires a very small C-band accelerator guide. The heat intensity of the accelerator guide is much higher than that of conventional S-band medical linear accelerators. The resonance frequency varies over almost 1.0 MHz with a thermal time constant of about 30 s. An automatic frequency controller (AFC) is employed to compensate for this variation in resonance frequency. Furthermore, we noted that fast AFC response is important for step-and-shoot intensity modulation radiotherapy (IMRT), in which the beam is turned on and off frequently. Therefore, we invented a digital AFC, based on a new concept, to provide effective compensation for the thermal characteristics of the accelerator guide and to ensure stable and optimized x-ray treatment. An important aspect of the performance of the AFC is the capture-frequency range over which the AFC can seek, lock on to, and track the resonance frequency. The conventional, analog AFC used in S-band medical linear accelerators would have a capture-frequency range of about 0.9 MHz, if applied to our accelerator guide, and would be inappropriate. Conversely, our new AFC has a capture-frequency range of 24 MHz, which is well suited to our accelerator guide. The design concept behind this new AFC has been developed and verified. A full prototype system was constructed and tested on an existing accelerator guide at the rated x-ray output (500 cGy/min) of our radiotherapy system, with a pulse-repetition frequency of 300 Hz. The AFC acquired the resonance frequency of the accelerator guide within 0.15 s after beam-on, and provided stable tracking and adjustment of the frequency of the microwave source to the resonance frequency of the accelerator guide. With a planned improvement of the initialization of the AFC it should be able to acquire the resonance frequency within 33 ms. © *2007 American Association of Physicists in Medicine.* [DOI: 10.1118/1.2752581]

Key words: automatic frequency control, AFC, C-band, linear accelerator, gimbaled x-ray head, 4D IGRT

I. INTRODUCTION

A new concept four-dimensional image-guided radiotherapy (4D IGRT) system[1] is under development. This system has an x-ray head composed of an ultrasmall C-band linear accelerator guide and a multileaf collimator (MLC) on gimbals mechanism. The gimbals mechanism is supported on a rotating O-ring structure, which provides isocentric motion for portal selection. Two axis angular motions of the gimbals provide active compensation for the mechanical distortion of the O-ring to attain beam positioning with a predicted accu-

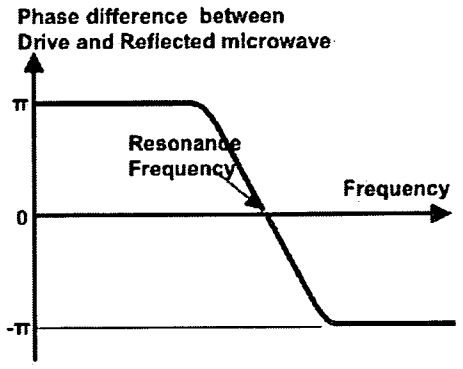

FIG. 1. The frequency dependence of the phase difference (P_d) between the drive microwave (P_{in}) and the reflected microwave (P_{ref}) of the standing wave type accelerator guide. In this figure, $P_d = P_{ref} - P_{in}$.

racy of ±0.1 mm and quick pursuit beam motions to compensate for respiratory and cardiac movements.

The accelerator guide is 38 cm in length and about 10 kg in weight.[2] The main acceleration structure is about 20 cm in length and about 4 kg in weight. The heat intensity is about 7 W/cm^3, or 0.65 W/g. After a cold start, the resonance frequency of the accelerator guide drifts downward by nearly 1.0 MHz from its cold-state (30°C) resonance frequency of 5712 MHz, over about 30 s.[2] If this drift in resonance frequency were not tracked properly (and the driving frequency of the high-power microwave source were not accurately controlled), in real time (so as to tune in to the resonance frequency), unacceptable variations of the beam energy and optics would be expected, and the characteristics of the treatment x ray would be variable and suboptimal.

Our 4D IGRT system is intended mainly for intensity modulation radiotherapy (IMRT). In step-and-shoot IMRT, in particular, the beam is turned on and off frequently, so that the delivered dose during one beam-on period will be as small as a couple of monitor units. One beam-on period will be less than 1 s, and the beam will be turned on and off hundreds of times during one fraction. Therefore, the drive frequency of the high-power microwave source must be tuned to the resonance frequency of the accelerator guide as soon as possible after beam-on. To effect a solution to this problem, an automatic frequency controller (AFC) is of prime importance in the control of the accelerator system; specifically, a very rapid, stable, and robust AFC is required.

All medical linear accelerators use an AFC[3] to stabilize the characteristics of the treatment x ray. The microwaves that are supplied to and reflected from the accelerator guide are both picked up by directional couplers with a low coupling coefficient, such as the Bethe hole coupler (BHC). These microwaves are mixed by a 3 dB hybrid coupler and converted into video signals by crystal detectors. The outputs of the crystal detectors are processed by a differential amplifier to control the frequency-tuning devices. In the case of a magnetron, its resonant cavity is mechanically driven by a servomotor until the magnetron reaches the frequency range in which it is forced to be in tune with the resonance frequency of the accelerator guide by the pulling effect of the

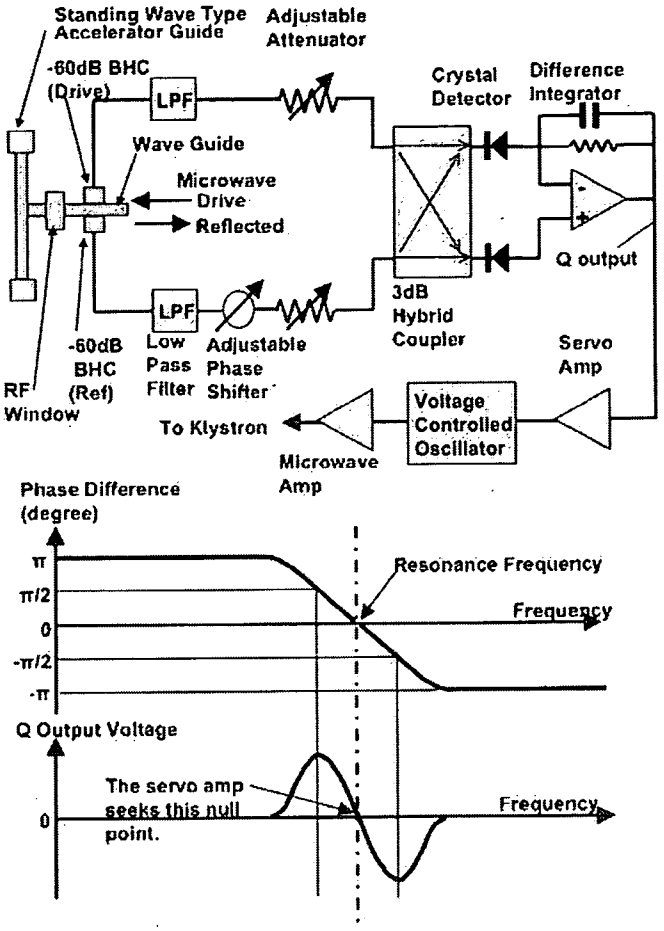

FIG. 2. The mechanization of the existing analog AFC for S-band medical linear accelerators. The microwaves that are supplied to and reflected from the accelerator guide are picked up by the BHC. These microwaves are mixed by a 3 dB hybrid coupler and converted into video signals by crystal detectors. The video signals are processed into Q output by the difference integrator. The Q output controls the frequency of the voltage controlled oscillator via the servo amp.

magnetron. In case of a klystron, the frequency of the klystron driver is electronically controlled by the output voltage of the differential amplifier.

However, all existing AFCs have a rather narrow capture-frequency range: the range over which the AFC can seek, lock on to, and track the resonance frequency of the accelerator guide in order to control the frequency of the microwave source. Existing AFCs are not suitable to our ultrasmall accelerator guide, whose resonant frequency varies rapidly over a wide range owing to its small heat capacity and its high heat density.

II. CONCEPT AND DESIGN

A. Concept

Figure 1 shows a typical relationship between the phase of the driving microwave (P_{in}) and the phase of the reflected microwave (P_{ref}) for a standing-wave type accelerator guide. The phase difference ($P_d = P_{ref} - P_{in}$) changes monotonically with the microwave frequency from π to $-\pi$, becoming zero at the resonance frequency of the accelerator guide, near

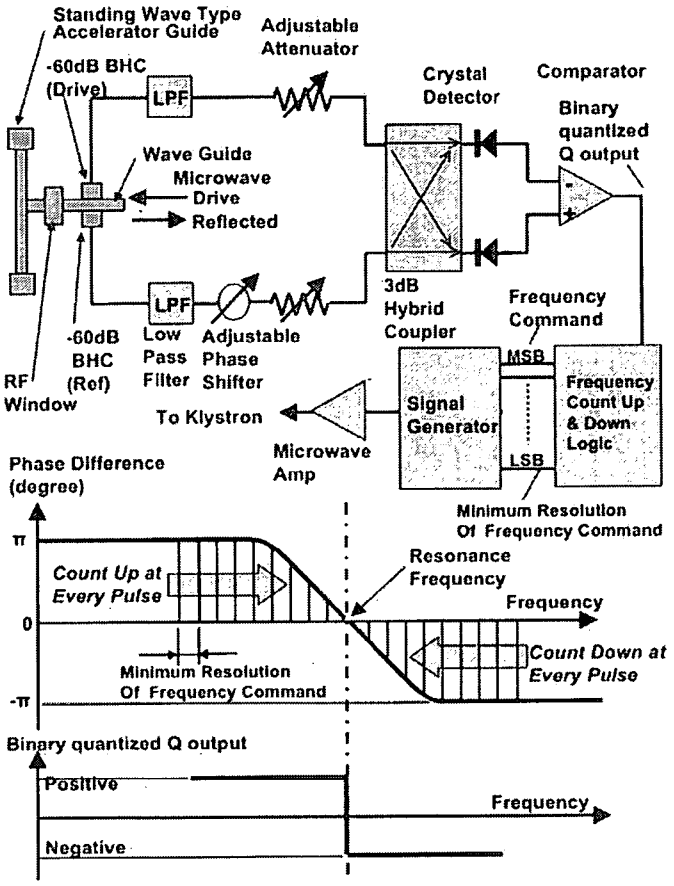

FIG. 3. The mechanization of our AFC. The microwaves that are supplied to and reflected from the accelerator guide are picked up by the BHC. These microwaves are mixed by a 3 dB hybrid coupler and converted into video signals by crystal detectors. The video signals are compared in the comparator and the binary quantized Q output (i.e., positive sign or negative sign of the Q output) is generated. The binary quantized Q output counts up or down the frequency command to the digitally controlled signal generator by one least-significant bit at every pulse. If the binary quantized Q output is positive, the frequency command is counted up, and if the binary quantized Q output is negative, the frequency command is counted down.

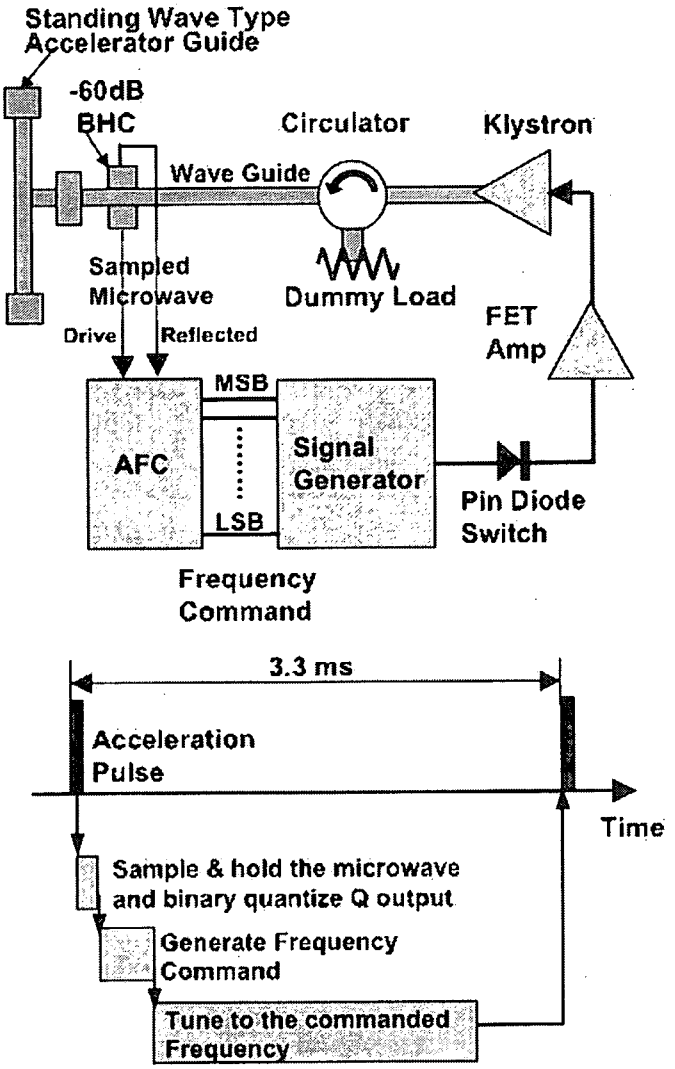

FIG. 4. The microwave block diagram and operational time chart for our accelerator system. MSB=most significant bit. LSB=least significant bit (corresponding to the resolution of the frequency command).

which it changes abruptly. This phase difference can be measured with a phase discriminator, which usually gives an in-phase (I) output of $\cos(P_d)$ and a quadrature (Q) output of $\sin(P_d)$.

A conventional AFC[2] controls the microwave frequency from the Q output as shown in Fig. 2. Essentially, the servo loop drives the microwave frequency so as to minimize the Q output. But, this control scheme works in a rather small frequency range ($-\pi/2 < P_d < \pi/2$) around the resonance frequency, as shown in Fig. 3, and the capturing frequency range is limited to less than 1.0 MHz around the resonance frequency.

On the other hand, our AFC uses only the sign of the Q output, as shown in Fig. 3. The Q output is binary quantized as either positive or negative, at every pulse. If the Q output has a positive sign, the microwave frequency is increased by one unit at the frequency resolution of the digitally controlled signal generator; if the Q output is negative, the microwave frequency of the signal generator is reduced by one unit of frequency resolution. If the settling time of the signal generator is sufficiently short, this process can be repeated at every pulse, effectively controlling the frequency of the signal generator at maximum resolution. This process may seem slow and awkward, but a detuned condition of 1 MHz can be compensated for within 0.17 s without any overshoot, if the resolution is 20 kHz and the pulse repetition frequency is 300 Hz. A resolution of 20 kHz is, therefore, sufficiently fine (3.5 parts per million) to be applied to a C-band accelerator guide. A pulse repetition frequency of 300 Hz yields a rated x-ray output of 500 cGy/min (in monitor units), with our system. Furthermore, the capture range is very wide and is limited only by the dynamic range of the quantizing circuit (namely, the comparator).

B. Details of the design

As shown in Fig. 4, our accelerator system uses a klystron as a high-power microwave source. The klystron driver is a solid state device composed of a signal generator, a pin diode switch for pulse shaping, and a field effect transistor (FET)

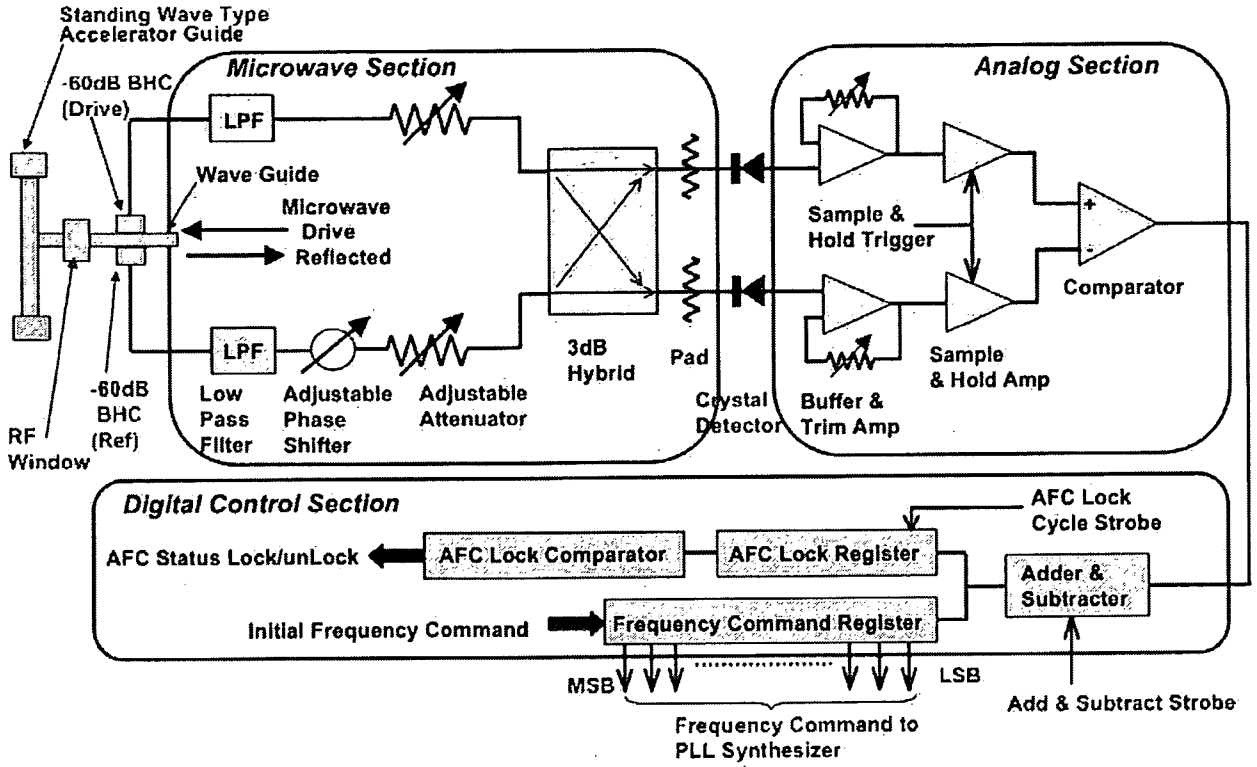

FIG. 5. Details of the new AFC. The drive and reflected microwave are picked up by the −60 dB BHC. These microwaves are conditioned through low pass filters (LPF), adjustable phase shifter, and adjustable attenuators and are input into the 3 dB hybrid coupler. The outputs of the 3 dB hybrid coupler are converted into video signals. The video signals are conditioned through the buffer and trim amps and sampled by the sample and hold amps. These sampled video signals are compared at the comparator. The positive or negative sign of the comparator output adds or subtracts the frequency command register by one least-significant bit.

amplifier. The signal generator is a crystal-controlled synthesizer with a phase-locked loop (PLL). The frequency is commanded, and the signal generator is tuned to the command frequency within 2 ms. The resolution of the command frequency is 20 kHz. After the PLL has locked and the frequency has settled, the pin diode switch shapes the microwave pulse, and the FET amplifier amplifies the pulsed microwave to a level sufficient to drive the klystron. The width of the microwave pulse is 5 μs, and the period between microwave pulses is about 3.3 ms at a pulse-repetition frequency of 300 Hz. The frequency can be commanded for each microwave pulse.

The detailed design of the AFC is shown in Fig. 5. The drive and reflected microwaves are picked up by the BHC at the input microwave port of the accelerator guide. The coupling coefficient of the BHC is −60 dB for both the drive and reflected microwaves. The picked up microwaves are conditioned through the low-pass filters (LPF), adjustable phase shifter, and adjustable attenuators, and pass into a 3 dB hybrid coupler. The outputs of the 3 dB hybrid coupler are converted into video signals by crystal detectors. The difference between these video signals is the Q output. Both video signals are acquired using sample-and-hold; they are fed into the comparator, whose output corresponds to the sign of the Q output. The comparator has a small dead zone around the zero-crossing point; above this dead zone the comparator gives a positive output, while below it the comparator gives a negative output. Within the dead zone, the comparator gives a zero output. If the comparator output is positive, the frequency command register is increased by one least-significant bit (LSB). If the comparator output is negative, the frequency command register is decreased by one LSB. If the comparator output is zero, the value of the frequency command resister is retained. One LSB corresponds to the minimum frequency resolution of 20 kHz. The AFC-lock register continuously averages the output of the adder and subtracter; if the value of the AFC register is below a particular value, the AFC is determined to be in a locked condition. The frequency command register controls the frequency of the signal generator. The value of the frequency command register represents the most recently measured resonance frequency of the accelerator guide. Furthermore, the frequency command register can be loaded with the estimated initial frequency value from an external controlling computer in order to further reduce the settlement time.

III. EXPERIMENTS, RESULTS, AND DISCUSSION

The performance of the AFC was evaluated with an existing C-band ultrasmall accelerator guide as shown in Fig. 5.

In preparation for the performance evaluation, the accelerator guide was operated at a 10 Hz pulse-repetition frequency and all adjustments were performed manually. The

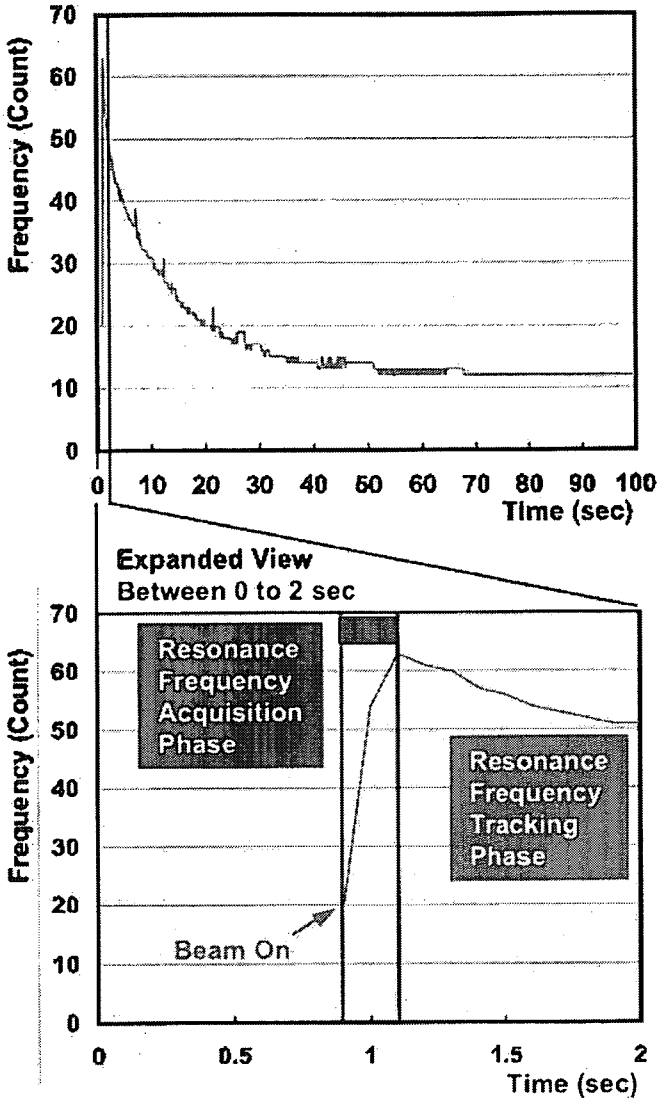

FIG. 6. The time history of the value of the frequency command register at the rated x-ray output. The pulse repetition frequency is 300 Hz. This register value corresponds to the resonance frequency of the accelerator guide.

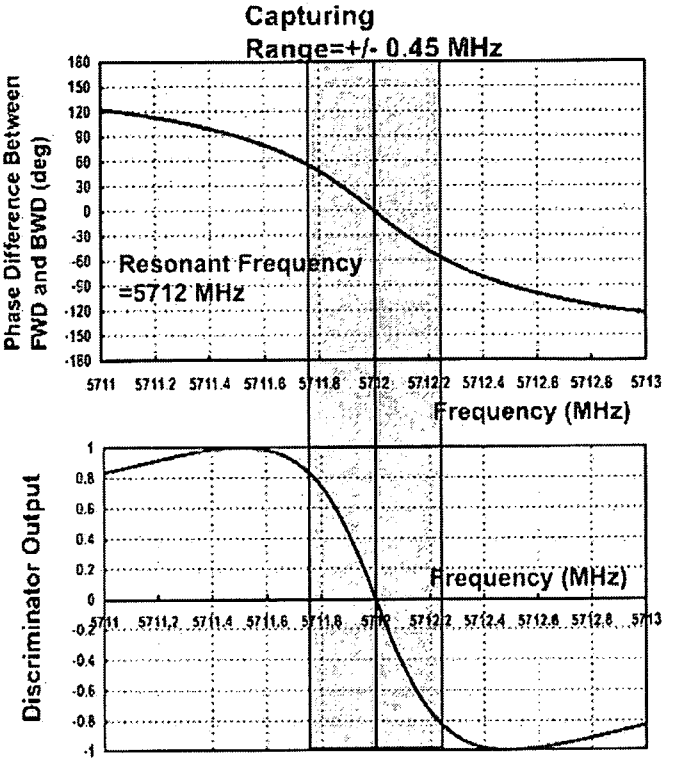

FIG. 7. The calculated capture frequency of the existing AFC when applied to our C-band accelerator guide.

adjustable attenuators and the buffer-and-trim amplifiers of the AFC were set to the correct values for optimizing the dynamic range of the buffer-and-trim amplifiers and the sample-and-hold amplifiers. The reflected power from the accelerator guide was divided from the BHC to be monitored, and the klystron drive frequency was adjusted manually so as to give the smallest reflected power (the tuned condition). The Adjustable phase shifter was adjusted to obtain zero output from the comparator at this klystron drive frequency.

The performance evaluation of the AFC was conducted with the accelerator guide started at a rated pulse-repetition frequency of 300 Hz, from the cold condition. The value of the frequency command register was monitored and represented as the klystron drive frequency.

Figure 6 shows the monitored value of the frequency-command register. The frequency is displayed as counts, where one count corresponds to 20 kHz. When the accelerator was started, the drive frequency was initially set to 20 counts. After the beam came on, the AFC sought and acquired the resonance frequency. At that time the resonance frequency of the accelerator guide was still that of the cold state and was higher by 43 counts (namely, 860 kHz). After acquiring the resonance frequency, the AFC tracked it stably and adjusted the klystron drive frequency. The resonance frequency decreased gradually along with the thermal expansion of the accelerator guide, and the steady state was reached about 50 s after the beam switched on. The spikes in the figure were found to arise from timing errors in the monitoring apparatus.

A. Settling time

The results show that it takes approximately 0.15 s to acquire the resonance frequency of the accelerator guide and that the AFC was able to completely track the resonance frequency. This implies that the settling time is 0.15 s.

If the control computer algorithm were to incorporate an expected accelerator guide resonance frequency, which it would initially provide to the AFC, the settling time would be considerably reduced. As the frequency command register of the AFC shows the most recently measured resonance frequency of the accelerator guide, the control computer should be able to estimate the resonance frequency within 10 counts (200 kHz), using the premeasured thermal time constant and the elapsed time from the latest beam-off period. In this case, the AFC would capture the resonance frequency within 10 pulses, and the settling time would be less than

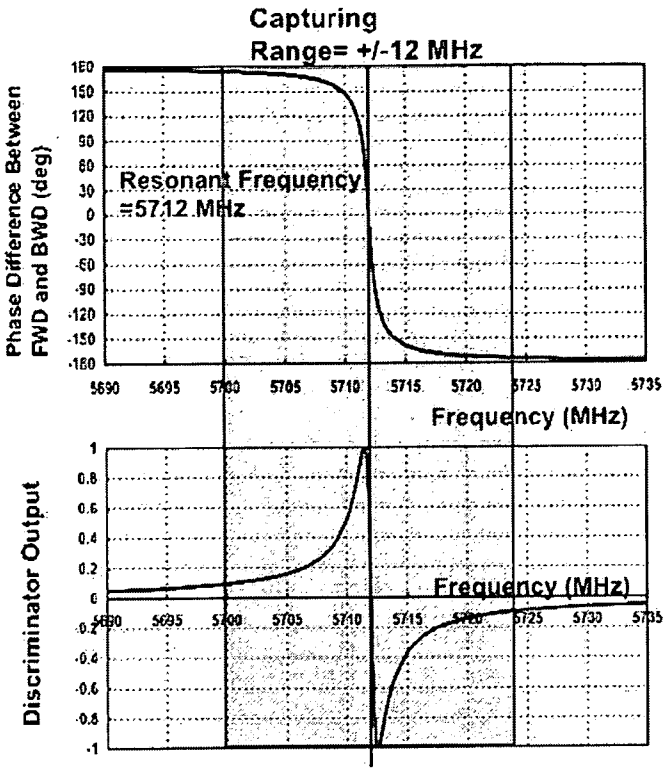

FIG. 8. The calculated capture frequency of our new AFC when applied to our C-band accelerator guide.

33 ms at a 300 Hz pulse repetition rate. Although detailed performance information of the AFCs in existing medical linear accelerators is not available, no analog AFC seems able to attain this level of performance.

B. Capture-frequency range

Figure 7 shows the predicted capture-frequency range of a conventional analog servo loop AFC if applied to our accelerator guide; Figure 8 shows that of our AFC. For our AFC, the dynamic range of the quantizing circuit (the comparator) is conservatively assumed to be 10 dB. The capture-frequency range of the existing analog servo loop AFC is ±0.45 MHz; this is inadequate for our accelerator guide, the resonant frequency of which changes through nearly 1 MHz. On the other hand, our AFC has a capture-frequency range of 24 MHz and can be applied to our accelerator guide with a favorable margin.

C. Robustness

An accelerator guide is an evacuated, high-power microwave device, and occasionally experiences voltage breakdown even after the commissioning period. The robustness of the AFC with respect to such a voltage breakdown event is important. With our AFC, the sign of the Q output at every pulse affects only the next pulse. Thus, a voltage breakdown of one pulse affects only the next pulse, causing a frequency change of one count (20 kHz). After the voltage breakdown is extinguished, the AFC immediately resumes resonance-frequency tracking, and the accelerator guide can be operated without any disruption. On the other hand, current AFCs will be affected by a large, abnormal Q output, the aftermath of which will continue during the time constant of the AFC servo loop, occasionally disrupting operation.

IV. CONCLUSIONS

A new design concept for an AFC has been established and developed to prototype stage. A system has been constructed and tested with an actual accelerator guide, at the rated x-ray output of 500 cGy/min, with a pulse-repetition frequency of 300 Hz. This new AFC acquired the resonance frequency of the accelerator guide within 0.15 s after beam-on, and provided stable tracking and adjustment of the frequency of the klystron.

The concept and design of the AFC proved to be adequate. With a proposed improvement to the initialization of the AFC, it should be able to acquire the resonance frequency within 33 ms.

The AFC is expected to have a much wider capture-frequency range (24 MHz) than that of any existing analog AFC. The AFC is also expected to be very robust against voltage breakdown events, favoring stable operation. The performance of an accelerator system incorporating this AFC will be reported in a later paper.

ACKNOWLEDGMENT

We are thankful for the assistance of Ichiro Yamashita of Mitsubishi Heavy Industries, Ltd. in the evaluation testing.

[a]Author to whom correspondence should be addressed. Electronic mail: yuichirokamino@nifty.com

[1]Y. Kamino, K. Takayama, M. Kokubo, Y. Narita, E. Hirai, N. Kawada, T. Mizowaki, Y. Nagata, T. Nishidai, and M. Hiraoka, "Development of a four-dimensional image-guided radiotherapy system with a gimbaled x-ray head," Int. J. Radiat. Oncol., Biol., Phys. 66, 271–278 (2006).
[2]Y. Kamino, S. Miura, M. Kokubo, I. Yamashita, M. Hiraoka, and J. Ishikawa, "Development of an ultrasmall C-band linear accelerator guide for a four-dimensional image-guided radiotherapy system with a gimbaled x-ray head," Med. Phys. 35, 1797–1808 (2007).
[3]C. J. Karzmark, C. S. Nunan, and E. Tanabe, *Medical Electron Accelerators* (McGraw-Hill, New York, 1993), pp. 102–104.